Article:
Ihli, J, Bots, P, Kulak, A et al. (2 more authors) (2013) Elucidating mechanisms of diffusion-based calcium carbonate synthesis leads to controlled mesocrystal formation. Advanced Functional Materials, 23 (15). 1965 - 1973. ISSN 1616-301X

https://doi.org/10.1002/adfm.201201742

Elucidating Mechanisms of Diffusion-Based Calcium Carbonate Synthesis Leads to Controlled Mesocrystal Formation

By *Johannes Ihli*, Pieter Bots, Alexander Kulak, Liane G Benning* and *Fiona C Meldrum**

[*] Professor Fiona Meldrum, Mr Johannes Ihli, Dr Alexander Kulak
School of Chemistry,
Woodhouse Lane,
Leeds, LS2 9JT, UK
Email: F.Meldrum@leeds.ac.uk

Professor Liane Benning, Dr Pieter Bots
School of Earth and Environment,
Leeds, LS2 9JT, UK

Keywords: Calcite • Mesocrystal • Biomineralization • Bio-Inspired • Biomimetic

Aggregation-based crystal growth often gives rise to crystals with complex morphologies which could not be generated via classical growth processes. Despite this, understanding of this mechanism is generally rather poor, particularly when organic additives or amorphous precursor phases are also present. In this paper, we take advantage of the observation that aggregation-based growth of calcium carbonate, and indeed many other minerals, is most often observed using diffusion-based synthetic methods. By fully characterizing the widely used ammonia diffusion method (ADM) – which is currently used as a "black box" – we have for the first time identified the solution and supersaturation conditions which accompany $CaCO_3$ precipitation using this method, and therefore gain insight into the nucleation and growth processes which generate calcite mesocrystals. This reveals that the distinguishing feature of the ADM is that the initial nucleation burst consumes only a minor quantity of the available ions, and the supersaturation then remains relatively constant, and well above the solubility of amorphous calcium carbonate (ACC), until the reaction is almost complete. New material is thus generated over the entire course of the precipitation, a feature which appears to be fundamental to the formation of complex, aggregation-based morphologies. Finally, the

importance of this understanding is demonstrated by using the identified carbonate and supersaturation profiles to perfectly replicate $CaCO_3$ mesocrystals through slow addition of reagents to a bulk solution. This approach overcomes many of the inherent problems of the ADM by offering excellent reproducibility, enabling the synthesis of such $CaCO_3$ structures in large-scale and continuous-flow systems, and ultimately facilitating *in situ* studies of assembly-based crystallization mechanisms.

1. Introduction

Significant efforts are made to synthesize crystals with defined sizes, morphologies and structures for applications in areas as wide-ranging as pharmaceuticals, biomaterials and nanomaterials.[1] In order to achieve control over these features it is necessary to understand the mechanisms by which crystals form. At one end of the spectrum, the classical picture of crystallization from solution envisages crystal growth to occur via ion-by-ion, or molecule-by-molecule addition to an established nucleus to give a single crystal product.[2] At the other, if growth of the individual nuclei is slow, then aggregation can dominate, leading to the formation of polycrystalline particles. Importantly, such aggregation-based processes often lead to crystalline particles with unusual morphologies, such as fibers,[3] and "microtrumpets"[4] which cannot be accessed through classical growth processes.

Aggregation-based crystal growth is currently receiving considerable interest.[2, 5, 6] While the formation of polycrystalline particles based on non-oriented aggregation of nanoparticles has been recognized for a long time, it was only in 1998 that Banfield and co-workers showed that single crystals of titania can form through the oriented aggregation of precursor nanoparticles,[7] a phenomenon they also observed in iron oxide systems,[8] and recently in the calcium sulfate system.[9] It is now well-established that many crystals grow by aggregation under appropriate experimental conditions, and that a number of mechanisms can operate, ranging from the oriented aggregation of crystalline nanoparticles to the

aggregation and then subsequent crystallization of amorphous nanoparticles.[5] While these processes can lead to single crystals indistinguishable from those formed by classical growth mechanisms, the crystals produced can also retain a memory of the precursor particles from which it forms. In this case, the crystal is classified as a mesocrystal, which ideally comprises a 3D array of iso-oriented single crystal particles of size 1–1,000 nm.[10] The ultrastructure of such a mesocrystal clearly contributes to defining its properties, as exemplified by sea urchin spines. These calcium carbonate single crystal biominerals have recently been classified as mesocrystals, where the nanoparticulate sub-structure and residual amorphous calcium carbonate may contribute to their remarkable mechanical properties.[10, 11]

Although aggregation-based growth promises the ability to produce crystals with unique morphologies and internal structures, this can only be achieved by elucidating the mechanisms by which aggregation occurs. Moving towards this goal, we here focus on calcium carbonate as an important mineral,[1, 12] which grows by aggregation under appropriate experimental conditions. Our approach is based upon the common observation that diffusion-based methods, including the double diffusion,[13, 14] the Kitano[15] and the ammonium carbonate diffusion method[16] often generate unusual crystal morphologies which cannot be accessed by other methods. This appears to be particularly true for additive-directed crystal growth, as exemplified by polymers such as poly(styrene sulfonate) or poly(4-styrenesulfonate-co-maleic acid) (PSS-co-MA), which have to-date only yielded calcium carbonate mesocrystals when using diffusion methods.[17-19]

This work characterizes the physico-chemical changes in solution which accompany $CaCO_3$ precipitation by the most widely used of these diffusion-based methods – the ammonium diffusion method (ADM) – where $CaCO_3$ precipitation is induced by exposing a solution of calcium ions to the vapor released on the decomposition of solid ammonium carbonate in a hermetically-sealed container (**Figure 1**).[16] This was achieved by performing time-resolved measurements of solution pH, carbon and calcium ion concentrations, and

identifying how these are determined by key variables including the Gas-Liquid interfacial area, the $CaCl_2$ concentration, the initial mass of ammonium carbonate, the stirring rate and the presence of a secondary diffusion barrier. A unique insight into the ADM is therefore generated by (i) identifying the variables which principally dictate the precipitation products and (ii) determining for the first time the carbon addition rates, and the supersaturation and reaction profiles.

To demonstrate the power of this understanding, we then use the identified carbon addition rates to reproducibly precipitate $CaCO_3$ mesocrystals in the presence of PSS-co-MA, through slow addition of reagents to a bulk solution. This provides an excellent "test" of our approach. The ability to prepare such $CaCO_3$ mesocrystals using alternative synthetic methods opens the door to industrial scale and potentially one-pot syntheses,[20] and will ultimately facilitate *in situ* studies of mesoscale assembly. Further, by identifying the solution conditions which give rise to $CaCO_3$ mesocrystals, we gain insight into their possible mechanisms of formation.

2. Results

2.1. General Description of the Ammonia Diffusion Method (ADM)

The ammonium diffusion method is characterized by two distinct steps, the first being the rapid saturation of the gas phase with CO_2 and NH_3 and the subsequent diffusion of the CO_2 and NH_3 molecules across the gas-liquid interface into the solution. In the slower, second step, the aqueous carbon dioxide reacts with the solution water to form carbonic acid, which in turn deprotonates in to both carbonate and bicarbonate ions, where the ratio of these species is defined by the solution pH. The dissolved NH_3, in turn, increases the pH of the solution. In combination with the calcium ions present, a solution that is supersaturated with respect to $CaCO_3$ is generated. The equations describing the solution equilibria are given in the Supporting Information.

The ADM was initially characterized from a standard set-up using 70 mL of 25 mM $CaCl_2$, with an air/solution surface area of 48 cm^2, 3 g of uncovered $(NH_4)_2CO_3$ and 2.6 L free volume in the reaction chamber. Time-resolved measurements were made of the key solution variables pH, calcium and carbonate concentration, which together yielded the carbon addition rates and underlying supersaturation profiles. Typical graphs showing the time-resolved changes in (A) turbidity (transmittance), (B) pH, (C) supersaturation, (D) calcium activity, (E) carbonate activity and (F) crystallization progress are presented in **Figure 2**. The turbidity measurements show a rapid decrease at ~15 mins (**Figure 2A**). This is likely caused by the formation of detectable calcium carbonate nuclei, thus revealing an induction period of 15 mins. The rapid drop in transmission after 15 min is associated with the formation of amorphous calcium carbonate (ACC) which subsequently transforms to vaterite and ultimately calcite, as confirmed by Raman and IR spectroscopy (**Figure S1**). The small increase in transmission at around 20 mins is observed in almost all experiments, and may result from the transition of ACC to a crystalline phase.[14, 24]

The turbidity measurements are also consistent with the pH data (**Figure 2B**). Knowledge of the solution pH is critical to understanding the ammonia diffusion method as it governs the distribution of aqueous carbonate speciation, and is required to determine the fraction of carbonate in the total carbon content measured.[22] A higher pH is associated with an increase in the concentration of carbonate at the expense of bicarbonate, and also promotes the dissolution of gaseous carbon dioxide into the $CaCl_2$ solution, through its conversion to bicarbonate or carbonate.[25] This process is reflected in the jump in supersaturation observed between 10 and 20 mins (**Figure 2C**). Nucleation of $CaCO_3$ therefore only occurs after a critical pH/ supersaturation has been reached (at pH~8.5), which marks the partial transformation of bicarbonate to carbonate. As shown in the data, this pH value is coincident with the induction point recorded using turbidity measurements. The pH then continues to increase until it reaches a value of ~9.8, where it remains rather constant ($CO_3^{2-}/HCO_3^- \approx 0.38$)

until the crystallization is almost complete. It then decreases very slowly to a constant value of ~9.2 after about 20 hours (**Figure S2**).

These data therefore indicate that in the ammonia diffusion method, initial ACC nucleation (at the induction point of ~ 15 mins) occurs above an ACC supersaturation threshold of > 10. Further, initial crystallization takes place under an excess of calcium ions, such that the ratio of calcium to carbonate ions is ~2.2. Comparison with alternative $CaCO_3$ precipitation methods therefore shows that the ADM results in initial ACC precipitation at relatively low supersaturation levels. Indeed, precipitation of ACC using the direct precipitation method,[24] (where 1 M calcium and carbonate solutions are combined and precipitation occurs after an induction period) occurs at S>100, while supersaturations of S >30 at pH > 12 are associated with Koga's method,[26] (where calcium and high pH carbonate solutions are combined giving immediate precipitation). As a further distinction between these different precipitation methods, the direct and Koga's method remove up to 90% of the total precipitation stress via the initial burst of ACC formation. In contrast, in the ADM the calcium and reaction profiles tend toward classical S shapes.

Following the onset of nucleation, the calcium ion profile undergoes an extended linear decrease due to its consumption in $CaCO_3$ precipitation (**Figure 2D**), while continued release of fresh ammonium carbonate vapour into the reaction chamber (which continues until equilibrium is reached after ~ 20 hrs) supports an increase in the solution carbonate concentration (**Figure 2E**). Consequently, the supersaturation continues to increase after the induction point until it peaks at its maximum value of ~180 between 60-80 mins under these reaction conditions. The supersaturation then decreases only very slowly, due to the continued introduction of carbonate into the solution. High supersaturation levels, which are well above the critical value for ACC, are therefore maintained even when a significant proportion of Ca^{2+} ions have been consumed. This prolonged period of high supersaturation is a key feature

of the ammonia diffusion method and would be expected to support multiple nucleation events.

2.2. Carbonate Addition Rate

Having identified the key features of the ADM, methods were developed to produce identical results using highly reproducible titration-based methods. This was achieved based on determination of the carbon addition rate (dC_T/dt). Here, C_T corresponds to the total inorganic carbon added to the system, which equals the sum of carbon lost to $CaCO_3$ precipitation and the total free inorganic carbon present in the solution (C_{TS}). The total carbon which has been added to the solution at any point in time (C_{TSt}) can be calculated from the reduction in the calcium ion concentration ($\Delta Ca = Ca_0 - Ca_t$), as determined by Atomic Absorption, and from the total carbon content in the solution ($\Delta C_{TS} = C_{TSt} - C_{TS0}$), as measured using Ion Chromatography, (Equation 2).

$$C_{T_t} = (C_{Ts_t} - C_{Ts_0}) + (Ca_0 - Ca_t) \qquad (2)$$

The carbon addition rate i.e. the rate at which carbon dioxide diffuses into the solution (dC_T/dt) is then obtained by differentiating Equation 2 with respect to time, to give Equation 3.

$$\frac{dC_T}{dt} = [C_{TS} - Ca]\frac{d}{dt} \qquad (3)$$

The experimental data (**Figures** 2 and **3**) shows that at times up to ≈ 100 mins (when the reaction is almost complete and the Ca concentration depleted) both the Ca and C_{TS} vary linearly with time, and that the pH is almost constant during the region of interest. The change in calcium and carbon concentration in solution can therefore be approximated using first order rate constants, $C_{Ts} = k_1t$, and $Ca = k_2t$, where t is the experimental time in minutes and k_1 and k_2 are rate constants corresponding to the carbon addition rate and the crystallization

rate respectively. Equation 3 can thus be expressed as Equation 4, where k_1 = 0.000634 mol L^{-1} min^{-1} and k_2 = - 0.000228 mol L^{-1} min^{-1}, based on the data presented in Figure 2.

$$\frac{dC_T}{dt} = k_1 - k_2 \qquad (4)$$

Graphs of the experimentally-obtained carbon addition profiles under the given "standard conditions" are presented in Figure 3, where (A) is the experimentally-obtained addition rate, (B) is theoretical, calculated using the derived rate constants k_1 and k_2, (**Table 1**) (C) is theoretical, calculated using k_1 only and (D) is experimental, based on diffusion of carbon dioxide into water rather than calcium chloride solution. The curves show that there is indeed a linear increase in the total carbon content until crystallization is virtually complete (at ≈ 100 mins). Further, this comparison demonstrates that the analysis made in Equation 4 well-describes the reaction in the first 100 mins under these standard conditions.

2.3. Influence of Reaction Variables

In describing the use of the ammonia diffusion method in the literature, authors typically place great weight on precisely defining variables such as the initial amount of ammonium carbonate, the calcium concentration, the solution surface area, the presence of further diffusion barriers and solution agitation. The effects of these variables were therefore investigated in order to determine their importance on the total carbon addition rate.

2.3.1. Initial Mass of Ammonium Carbonate.

Provided that the initial amount of solid ammonium carbonate was in excess, the precise mass used in an experiment had no influence on the precipitation profile. This is shown in the total carbon addition rates, dC_T/dt, which were identical when either 1.5 g, 3 g or 5 g of ammonium

carbonate were employed (Table 1 and **Figure S3**). This result confirms that a near-constant vapour pressure is present.

2.3.2. Initial Calcium Concentration

The initial calcium concentration, by contrast, had some effect on the precipitation reaction, although the crystallization progress was little affected. Increasing the initial calcium concentration from 10 mM to 50 mM unexpectedly resulted in shifts in the induction point and pH profile to longer times (**Figure 4**), although there was little change of the plateau pH value. This may result from the accompanying increase in the concentration of chloride ions, which could lead to the formation of ammonium chloride complexes. This would retard the increase in pH and therefore the transformation of bicarbonate to carbonate.

The most significant effect of changing the calcium concentration was on the supersaturation. The supersaturation levels at induction decreased with decreasing calcium concentration due both to the lower calcium concentration and the lower levels of bicarbonate present at induction. On progression of the reaction, significantly higher supersaturation levels of ≈ 230 are reached in the 50 mM solution, as compared with ≈ 75 in the 10 mM solution, which can be associated with a higher nucleation density as the calcium concentration is raised. Characterization of the reaction products sampled after 100 mins using SEM and Raman microscopy showed that the Ca concentration also influenced the polymorph produced, and that a greater proportion of vaterite to calcite was obtained at 10 mM as compared with 50 mM (**Figures S4** and **S5**). The carbon addition rate also increased with the initial calcium concentration due to increased $CaCO_3$ precipitation, resulting in an extended period of high CO_2 diffusion into the solution, as shown in Table 1 and **Figure S6**.

2.3.3. Initial Calcium Concentration

Variation of the solution surface area, while maintaining a constant volume, resulted in significant and systematic changes in all of the parameters investigated, indicating that this provides an excellent and straightforward method for controlling the diffusion process (**Figures 5 and S7**). Induction times decreased with increasing surface areas, while more rapid increases in the pH and associated nucleation rates were observed at higher surface areas. This is expected due to the more uniform supersaturation profiles in solutions with larger surface areas. Figure 5 confirms the linearity of this relationship, which is in agreement with Fick's first law,[27] i.e. doubling the surface area leads to a twofold increase in carbon addition rate. Similarly, the reaction progress increased with increasing surface area, and the supersaturation peaked at earlier times in the more rapid (larger surface area) reactions. Therefore, larger surface areas are associated with shorter induction and overall reaction times, higher peak supersaturations, and nucleation rates. In contrast, the lower surface area provides conditions where supersaturations are maintained at constant values for long periods.

2.3.4. Diffusion Barriers.

Introduction of an additional diffusion barrier (typically in the form of Parafilm perforated with needle-holes) is widely used as a method of regulating the ADM. Experiments were therefore conducted where the dish containing the reaction solution was covered with Parafilm punctured with 3, 10 or 20 holes, corresponding to a total free area of 0.6, 2 and 4 cm^2 respectively. A decrease in the rate of calcium loss and in the reaction progress was observed with a reduction in the free area, and the induction time increased from ~ 15 mins in the absence of a diffusion barrier to ~ 100 mins when there was only 0.6 cm^2 free area. However, in both of these cases, nucleation occurred at supersaturations above the ACC solubility limit, (Table 1). The total carbon addition rate was found to exponentially decrease with a decrease in the free area, in contrast to the linear relationship recorded with respect to

the liquid surface area. Thus, in common with a reduction in the solution surface area, reduction in the free area through introduction of a diffusion barrier leads to longer reaction times, where supersaturation remains at elevated levels for longer periods.

2.3.5. Stirring

The effect of agitation on the ADM was studied by addition of a magnetic stirrer to the $CaCl_2$ solution. An influence on the crystallization was only observed at stirring rates of 100 rpm and above, where a higher crystallization rate was recorded as compared with unstirred solutions (**Figure 6**). The effect of stirring was more pronounced in the later stages of crystallization, and no significant change in the induction time was observed, despite there being a more rapid initial increase in the pH (**Figure S8**). This is consistent with a faster build-up in ammonia and carbonate in the solution, and nucleation occurring at higher supersaturations in the stirred solutions. The increase in reaction rate in the later stages of the reaction can be explained by an increase in secondary nucleation events which occurs due to an increased frequency of particle collisions, the generation of additional nucleation sites through attrition processes, and the increased kinetic energy in the system. It is also supported by the presence of aragonite as well as calcite under stirred conditions, while only calcite is present under stagnant conditions (Figure S4). The formation of aragonite due to agitation has been reported elsewhere,[28] and may relate to the increase of kinetic energy in the system.

2.4. Reproduction of the Ammonia Diffusion Method

$CaCO_3$ mesocrystals formed in the presence of PSS-MA were chosen as a model system to test the translation of the obtained ADM reaction conditions to a titration-based system, due to their distinctive morphologies and properties (in particular their high surface areas of 60-100 m^2/g). Success in the replication of mesocrystals is particularly important as it provides

support for our analysis which suggests that a prolonged, steady supersaturation promotes the continuous formation of new material, which supports aggregation-based crystallization.

Here, a carbonate containing reagent solution (20 mL of either 250 or 175 mM $(NH_4)_2CO_3$) was added at 0.0057 mL/min to a 80 mL of solution containing 325 ppm PSS-MA and either 5 mM or 1.25 mM $CaCl_2$, under agitation at 70 rpm. The experimental conditions were selected to mimic the carbon addition rate during the crystallization zone (the first 100-200 mins of reaction) of an ammonium carbonate diffusion reaction with the following conditions: 5 mM /1.25 mM $CaCl_2$, 325 ppm PSS-MA, 70 mL, 48 cm^2 and 0.6 cm^2 diffusion boundary pore surface area. The ammonium carbonate solution addition rate (k_S) and concentration ($C(NH_4)_2CO_3$) added to a certain volume of calcium solution (V_{Ca}) were determined according to Equation 5 such that they mimicked the carbon addition rate (dC_T/dt) obtained experimentally from characterization of the ADM.

$$\frac{k_S\, C_{(NH_4)_2CO_3}}{V_{Ca} + k_L t} = \frac{dC_T}{dt} \qquad (5)$$

Characterization of the product crystals demonstrated that they were calcite, as shown by Raman and IR Spectroscopy (**Figure S9**), and that they were either pseudo-octahedral or dodecahedral in morphology (**Figures 7A** and **7B**). Importantly, these morphologies were identical to those of the $CaCO_3$ mesocrystals produced using the ADM (**Figures 7C** and **7D**). Further confirmation of mesocrystal structure was obtained by measurement of the surface areas of the crystals. Analysis of pseudo-octahedral mesocrystals produced by slow addition, and removed from the reaction solution after 12 hr, revealed typical surface areas of ~ 97 m^2/g. This value is consistent with the corresponding crystals produced using the ADM,[17] (~82 m^2/g) and is considerably larger than the 1-2 m^2/g recorded for rhombohedral calcite crystals

of comparable sizes. Thermogravimetric analysis (TGA) of the "replica" mesocrystals revealed that they comprised 2-4 wt% polymer (**Figure S10**).

3. Discussion

A number of studies have previously attempted to either modify, or characterize features of the ammonia diffusion method in order to achieve greater reproducibility. These have included substitution of solid ammonium carbonate with a liquid reservoir of ammonium carbonate,[29, 30] or estimation of pH and supersaturation changes (while neglecting precipitation) for precipitation in μL droplets in a so-called crystallization mushroom.[30] A general comparison of the ammonia diffusion and double diffusion methods has also been made by studying the pH profile.[31] By comparison, our approach provides a very detailed picture of the changes in solution which accompany the precipitation of $CaCO_3$ using the ADM.

The results presented here demonstrate that the ADM can be controlled using a range of variables including the introduction of a diffusion barrier, and change of the solution surface area, which leads to modification of the reaction profile. Where conditions are used which lead to a rapid reaction rate, the reaction profile and solution conditions approach those achieved in other techniques. This is characterized by a burst of nucleation which depletes a large proportion of the available calcium ions, followed by a steady drop in the supersaturation as the nuclei grow in solution. In contrast, when the ADM conditions are controlled to give slow growth, a unique profile can be generated where nucleation occurs in an initial burst, which consumes only a relatively small proportion of the available ions, and the supersaturation then remains relatively constant, at a level well above the threshold for amorphous calcium carbonate (ACC) precipitation, until the calcium ions have been depleted. It is the precipitation of $CaCO_3$ crystals under the latter conditions that can lead to the

generation of unique and often complex crystal morphologies when organic additives such as block copolymers are also present in the reaction solution.

Identification of the solution conditions which lead to these complex crystal structures – which determine the nucleation and growth processes which could feasibly occur – therefore provides a unique insight into the processes which may generate such crystals. As the precipitation occurs under conditions where the supersaturation remains constant, but at a level above the ACC threshold for the vast majority of the reaction, it is possible for new nuclei to form throughout the reaction, probably as ACC. This may occur homogeneously or heterogeneously on existing nuclei in solution. If further nucleation does not occur, the nuclei formed in the original nucleation event will simply continue to grow. These nucleation and growth processes may of course also occur in tandem.

In the absence of polymer additives, calcite rhombohedra are the typical products of the ADM both under slow and rapid growth regimes. Studies of ACC precipitation in bulk solution (achieved by mixing solutions or calcium and carbonate ions) have shown that ACC particles form in a nucleation burst, and then continue to grow without aggregation.[32] The mechanism by which they crystallize is less clear. It has been suggested that nucleation of the crystalline phase occurs homogeneously,[33] and there is strong evidence that growth of the crystalline nuclei then occurs via dissolution/ reprecipitation.[34] Further, an ACC particle cannot start to crystallize until it reaches a critical size.[35] Crystallization of ACC to vaterite in bulk solution via a solid state transformation has also been suggested, based on SAXS/WAXS studies.[24] The ACC nanoparticles were believed to first dehydrate, then undergo a structural rearrangement to vaterite, and finally aggregate to form micron-scale vaterite particles.

This process will obviously be modified in the presence of polymers, which are likely to bind to the ACC particles, inhibiting their growth and potentially promoting aggregation. Some studies have attempted to characterize the mechanism of formation of $CaCO_3$

mesocrystals in the presence of polymer additives. These have analyzed the reaction solutions at early times using transmission electron microscopy (TEM), analytical ultracentrifugation and dynamic light scattering,[19, 36, 37] and have shown the presence of amorphous nanoparticles at early reaction times. As a particular feature of polymer-controlled growth, which distinguishes it from additive-free reactions, these ACC particles rapidly form aggregates, which then ultimately crystallize. Given the challenging nature of these early-time studies, they present only a broad picture of the reaction processes, and little is known about the growth of the aggregates or their crystallization mechanism.

Our results are therefore fully in keeping with these observations, but importantly also demonstrate that under slow growth in the ADM – which is the regime where mesocrystals are observed – new material is continually produced after the initial nucleation of ACC. This then distinguishes it from rapid growth conditions where there is a single nucleation event, followed by growth. The most probable scenario is therefore that new particles nucleate on the existing polymer-stabilized ACC aggregates, or on crystalline particles at later stages of the reaction, giving rise to more complex morphologies.

The formation of $CaCO_3$ mesocrystals would therefore therefore appear to be based on the crystallization of an assembly of ACC nanoparticles rather than the oriented assembly of precursor crystalline nanoparticles as was originally suggested.[19, 36] Indeed, nanoparticulate calcite and vaterite are very hard to synthesize due to their rapid growth in solution. In this way, synthetic $CaCO_3$ mesocrystals would appear to have many similarities to biogenic calcite mesocrystals, where the ultrastructure derives from a memory of the ACC precursor phase.[10] It is also stressed that Ostwald ripening processes are active during $CaCO_3$ precipitation, such that large crystals grow at the expense of smaller ones. Indeed, it is noted that under even the slowest reaction times used here, the reaction is complete and the calcium ions depleted after 6-8 hrs. Therefore, while a number of articles describe the precipitation of $CaCO_3$ crystals using the ADM using prolonged incubation periods (days to weeks), any morphological

changes reported in crystals after ≈ 12 hrs are simply due to Ostwald ripening/ recrystallization processes. Given that polymer remains in the solution, rough crystal surfaces, as seen in $CaCO_3$ mesocrystals would be expected.

4. Conclusions

Although the ammonium diffusion method is widely used to precipitate calcium carbonate, due in part to its ability to generate unique crystal morphologies, it is typically used as a "black box" with little or no understanding of the supersaturation levels or changes in solution which accompany crystallization. In this work, we have addressed this challenge and have provided a rigorous characterization of the ADM. This approach has enabled identification of the key solution conditions which give rise to these morphologies, and has shown that the distinguishing feature of the ADM is that the initial nucleation burst consumes only a relatively small amount of the available ions, and the supersaturation then remains relatively constant, and well above the threshold value for ACC, until the majority of the calcium ions have been consumed. New material is therefore generated throughout the course of the precipitation reaction, a feature which we believe to be fundamental to the formation of complex, aggregation-based morphologies. This understanding of the ADM enables control over the process, and has also facilitated development of a simple, slow addition-based synthesis method which can replicate $CaCO_3$ mesocrystal morphologies. This new technique overcomes the inherent irreproducibility of the ADM, and provides great flexibility, enabling for example scale-up of the process, and the possibility of establishing a continuous crystallizer setup. Finally, although the focus of the study has been $CaCO_3$, it is expected that the solution conditions which promote aggregation-based crystal growth are likely to be quite general, such that it will be possible to use the insight gained here to control the crystallization of many materials.

5. Experimental Section

A full description of all methods and calculations used is provided in the Supporting Information, supported by an overview of key methods here.

5.1. Characterization of the Ammonium Diffusion Method (ADM)

A crystallization dish containing calcium chloride solution was placed in a desiccator, and a pH electrode, a temperature recorder and tube through which sample aliquots could be removed were inserted into the solution (Figure 1). This dish was either uncovered, or was covered with perforated Parafilm to provide a secondary diffusion barrier. Solid ammonium carbonate, spread in a glass dish, was added to the chamber, which was then sealed. The changes in the reaction solution accompanying precipitation of $CaCO_3$ were then evaluated by taking samples from the solution at key time points, and quenching them to prevent further reaction. The solution was then separated from the solid matter by centrifugation, and the total concentrations of aqueous calcium containing species and carbon present were determined using atomic absorption spectroscopy (AA) and Ion chromatography (IC) respectively. The weight loss of the ammonium carbonate during the reaction was also determined. In a second set of experiments, the above setup was extended to determine the induction point by recording changes in the solution turbidity with time using UV-Vis spectroscopy [21].

5.2. Calculation of Carbonate Concentration, Supersaturation and Crystallization Progress

The solution carbonate concentrations (CO_3^{2-}, HCO_3^- and H_2CO_3) were calculated, based on the total inorganic carbon concentration (C_{TS}) and pH measured, [22] using a simplified carbon mass balance and carbonic dissociation constants (K_A). The crystallization progress (ξ) was determined by recording the total calcium concentration in solution, as described in Equation 1 [23].

$$\xi = \left(\frac{Ca_t - Ca_i}{Ca_t - Ca_{equilibirum}} \right) \quad (1)$$

The calculated supersaturation (S) with respect to a specific polymorph (x), was expressed as the ratio of ionic activity product to solubility product (K_{sp}).

5.3. Precipitation of Calcium Carbonate Mesocrystals

In order to test whether the characterization of the ADM carbonate and supersaturation profiles could be translated to a diffusion-free experimental set-up, $CaCO_3$ mesocrystals were precipitated in the presence of poly(4-styrenesulfonic acid co-maleic acid) (PSS-MA) by mechanical slow addition of reagents into solution under conditions which paralleled the ADM. The crystal morphologies were then compared with those prepared from identical reagents using the ADM. Replication of the ADM was achieved by slow addition of a $(NH_4)_2CO_3$ solution into a crystallization dish containing a$CaCl_2$-PSS MA solution using a syringe pump, where the system was under constant agitation with an orbital shaker. The addition rate and concentration of the $(NH_4)_2CO_3$ were determined based on the carbon addition rates derived from the ADM. The surface area of the $CaCO_3$ mesocrystals produced was determined using the method of Brunauer, Emmett and Teller (BET) while Thermogravimetric analysis (TGA) was applied to determine the polymer content in the crystals. Crystal morphologies were characterized using SEM and crystal polymorphs were determined by Raman microscopy. As a control, $CaCO_3$ mesocrystals were also precipitated using the traditional ADM, carried out as described in Section 5.1.

Acknowledgements

We thank the EPSRC for financial support *via* grant EP/H005374/1 (JI and FCM). The work was also supported by the European Union "Mineral Nucleation and Growth Kinetics (MIN-

GRO) Marie-Curie Research and Training Network", Grant MRTNCT-2006-035488. David Ashley is acknowledged for his assistance with ion chromatography measurements. Supporting Information is available online from Wiley InterScience or from the author.

[1] F. C. Meldrum, H. Colfen, Chem. Revs. **2008**, 108, 4332.

[2] R. Q. Song, H. Colfen, Crystengcomm **2011**, 13, 1249.

[3] S. H. Yu, H. Colfen, K. Tauer, M. Antonietti, Nat. Mater. **2005**, 4, 51; Y. Y. Kim, A. N. Kulak, Y. T. Li, T. Batten, M. Kuball, S. P. Armes, F. C. Meldrum, J. Mater. Chem. **2009**, 19, 387.

[4] C. Viravaidya, M. Li, S. Mann, Chem. Commun. **2004**, 2182.

[5] R. Q. Song, H. Colfen, Adv. Mater. **2010**, 22, 1301.

[6] Q. Zhang, S. J. Liu, S. H. Yu, J. Mater. Chem. **2009**, 19, 191; V. M. Yuwono, N. D. Burrows, J. A. Soltis, R. L. Penn, J. Am. Chem. Soc. **2010**, 132, 2163.

[7] R. L. Penn, J. F. Banfield, Science **1998**, 281, 969.

[8] J. F. Banfield, S. A. Welch, H. Z. Zhang, T. T. Ebert, R. L. Penn, Science **2000**, 289, 751.

[9] A. E. S. Van Driessche, L. G. Benning, J. D. Rodriguez-Blanco, M. Ossorio, P. Bots, J. M. Garcia-Ruiz, Science **2012**, 336, 69.

[10] J. Seto, Y. R. Ma, S. A. Davis, F. Meldrum, A. Gourrier, Y. Y. Kim, U. Schilde, M. Sztucki, M. Burghammer, S. Maltsev, C. Jager, H. Colfen, Proc. Nat. Acad. Sci. **2012**, 109, 3699.

[11] Y. Oaki, A. Kotachi, T. Miura, H. Imai, Adv. Func. Mater. **2006**, 16, 1633.

[12] L. B. Gower, Chem. Revs. **2008**, 108, 4551.

[13] Y. Y. Kim, N. B. J. Hetherington, E. H. Noel, R. Kroger, J. M. Charnock, H. K. Christenson, F. C. Meldrum, Angew. Chem. Int. Ed. **2011**, 50, 12572.

[14] E. Loste, R. J. Park, J. Warren, F. C. Meldrum, Adv. Func. Mater. **2004**, 14, 1211.

[15] Y. Kitano, K. Park, D. W. Hood, J. Geophys. Res. **1962**, 67, 4873.

[16] J. Aizenberg, S. Albeck, S. Weiner, L. Addadi, J. Cryst. Growth **1994**, 142, 156; S. Albeck, S. Weiner, L. Addadi, Chem. Eur. J. **1996**, 2, 278.

[17] R. Q. Song, H. Colfen, A. W. Xu, J. Hartmann, M. Antonietti, Acs Nano **2009**, 3, 1966.

[18] A. N. Kulak, P. Iddon, Y. T. Li, S. P. Armes, H. Colfen, O. Paris, R. M. Wilson, F. C. Meldrum, J. Am. Chem. Soc. **2007**, 129, 3729.

[19] T. X. Wang, H. Colfen, M. Antonietti, J. Am. Chem. Soc. **2005**, 127, 3246.

[20] M. Faatz, F. Gröhn, G. Wegner, Adv. Mater. **2004**, 16, 996.

[21] Y. W. Wang, Y. Y. Kim, C. J. Stephens, F. C. Meldrum, H. K. Christenson, Cryst. Growth Des. **2012**, 12, 1212.

[22] H. L. Bohn, B. McNeal, G. O'Connor, in *Soil Chemistry*, John Wiley Sons, **1985**, 316.

[23] M. Donnet, P. Bowen, J. Lemaitre, J. Coll. Int. Sci. **2009**, 340, 218.

[24] P. Bots, L. G. Benning, J.-D. Rodriguez-Blanco, T. Roncal-Herrero, S. Shaw, Cryst. Growth Des. **2012**, DOI: 10.1021/cg300676b.

[25] H. V. Tran, L. D. Tran, H. D. Vu, H. Thai, Coll. Surf. A **2010**, 366, 95.

[26] N. Koga, Y. Nakagoe, H. Tanaka, Thermochim. Acta **1998**, 318, 239.

[27] A. Fick, Annal. Phys. **1855**, 170, 59.

[28] B. Aziz, D. Gebauer, N. Hedin, CrystEngComm **2011**, 13, 4641.

[29] M. G. Page, H. Cölfen, Cryst. Growth Des. **2006**, 6, 1915.

[30] J. Gomez-Morales, A. Hernandez-Hernandez, G. Sazaki, J. M. Garcia-Ruiz, Cryst. Growth Des. **2010**, 10, 963.

[31] A. Becker, W. Becker, J. C. Marxen, M. Epple, Zeit. Anorg. Allg. Chem. **2003**, 629, 2305.

[32] D. Pontoni, J. Bolze, N. Dingenouts, T. Narayanan, M. Ballauff, J. Phys. Chem. B **2003**, 107, 5123; J. Bolze, B. Peng, N. Dingenouts, P. Panine, T. Narayanan, M. Ballauff, Langmuir **2002**, 18, 8364; J. Liu, S. Pancera, V. Boyko, A. Shukla, T. Narayanan, K. Huber, Langmuir **2010**, 26, 17405.

[33] E. M. Pouget, P. H. H. Bomans, J. Goos, P. M. Frederik, G. de With, N. Sommerdijk, Science **2009**, 323, 1455; C. J. Stephens, Y. Y. Kim, S. D. Evans, F. C. Meldrum, H. K. Christenson, J. Am. Chem. Soc. **2011**, 133, 5210.

[34] K. Sawada, Pure Appl. Chem. **1997**, 69, 921; J. R. I. Lee, T. Y. J. Han, T. M. Willey, D. Wang, R. W. Meulenberg, J. Nilsson, P. M. Dove, L. J. Terminello, T. van Buuren, J. J. De Yoreo, J. Am. Chem. Soc. **2007**, 129, 10370; T. Y. J. Han, J. Aizenberg, Chem. Mater. **2008**, 20, 1064.

[35] C. C. Tester, R. E. Brock, C. H. Wu, M. R. Krejci, S. Weigand, D. Joester, Crystengcomm **2011**, 13, 3975; F. Nudelman, E. Sonmezler, P. H. H. Bomans, G. de With, N. A. J. M. Sommerdijk, Nanoscale **2010**, 2, 2436.

[36] A. W. Xu, M. Antonietti, H. Colfen, Y. P. Fang, Adv. Func. Mater. **2006**, 16, 903.

[37] R. Q. Song, A. W. Xu, M. Antonietti, H. Colfen, Angew. Chem. Int. Ed. **2009**, 48, 395.

Received: ((will be filled in by the editorial staff))
Revised: ((will be filled in by the editorial staff))
Published online: ((will be filled in by the editorial staff))

Figure 1. Schematic diagram of the experimental set-up and methods used to determine the concentrations of aqueous Ca^{2+} and CO_3^{2-} ions; Timely sample aliquots were removed and quenched with ethanol, the [Ca^{2+}] was determined using atomic absorption (AA), and the [CO_3^{2-}] using ion-chromatography (IC).

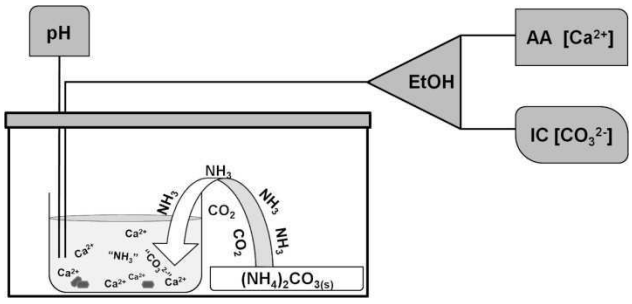

Figure 2. Time-resolved profiles of calcium carbonate precipitation using the ADM, with reaction conditions: 25 **mM** $CaCl_2$, 70 mL, 3 g ammonium carbonate, 2.6 L reaction chamber, no additional diffusion boundaries. The data shown are averages of three experiments, and the error bars show the standard deviation in the values. (A) Transmission, (B) pH, (C) Supersaturation, (D) Calcium activity, (E) Carbonate activity, (F) Crystallization progress.

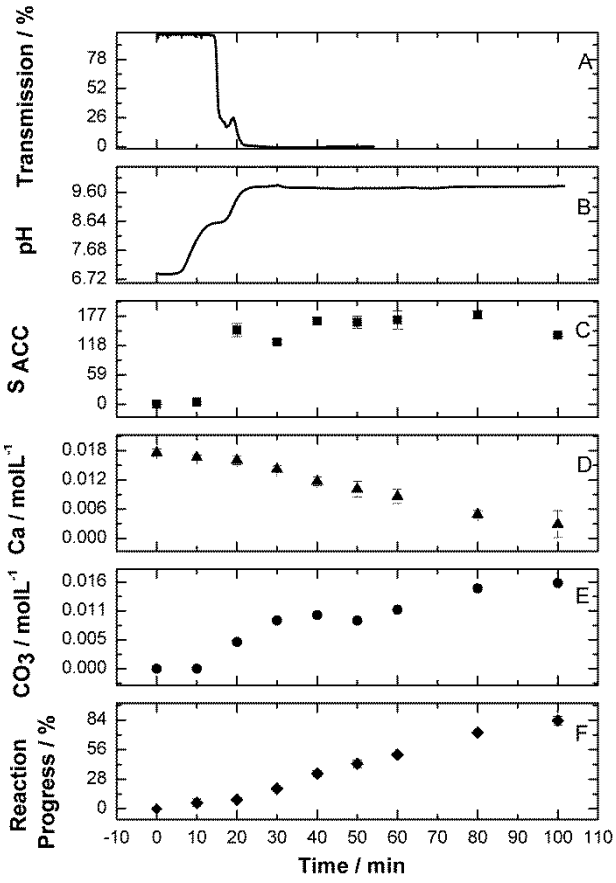

Figure 3. Comparison of Total Carbon addition rates, (A) Experimental, (B) Theoretical (C) Theoretical k_1 only, (D) Experimental pure diffusion no calcium chloride.

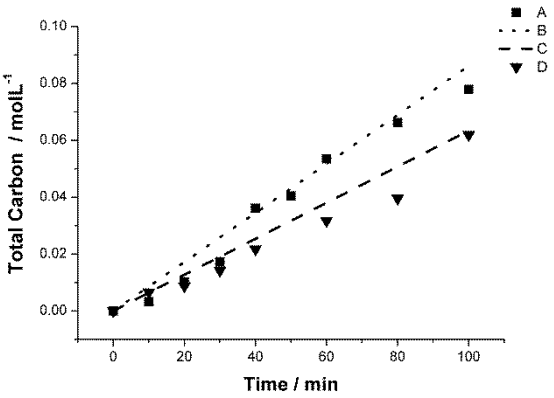
A
B
C
D
Total Carbon / molL-1
0.10
0.08
0.06
0.04
0.02
0.00
0
20
40
60
80
100
Time / min

Figure 4. Graphs showing the influence of the initial calcium concentration on the induction point (as measured by the transmittance), the pH profile and the supersaturation. — 10 mM $CaCl_2$, - - • 25 mM $CaCl_2$, - • - 50 mM $CaCl_2$. The data shown are an average of three experiments.

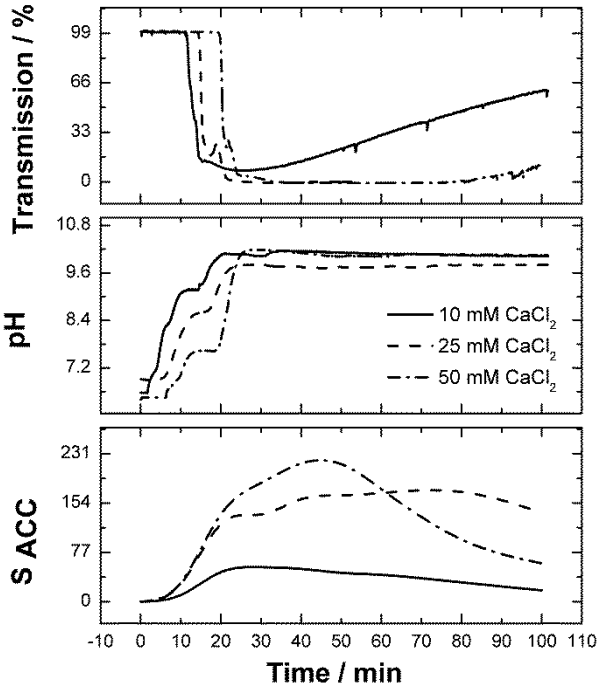

Figure 5. Graphs of the influence of the solution surface area on the pH profile, supersaturation and total carbon added ● / ••• 13 cm^2-, ▲/ - - 48 cm^2-, ■/ — 58 cm^2- 25 mM $CaCl_2$. The data shown are an average of three experiments.

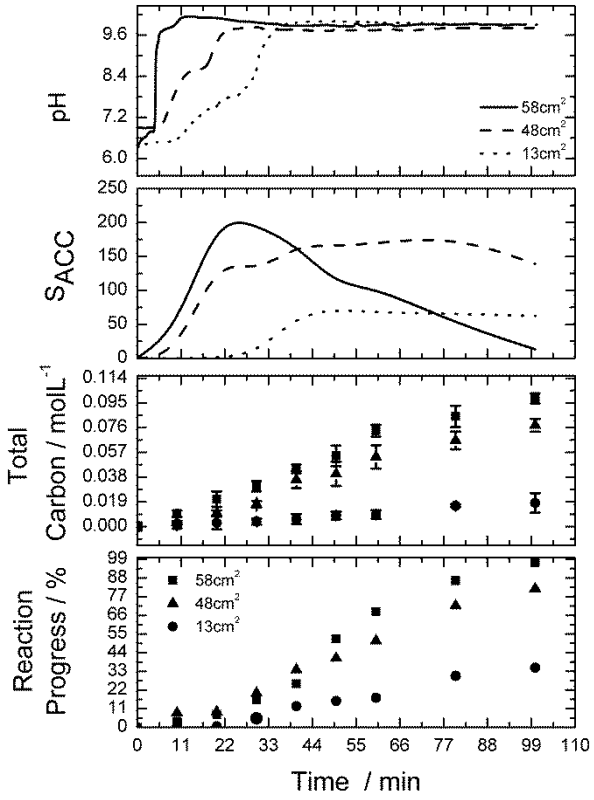

Figure 6. Graphs showing the influence of solution agitation on the supersaturation and reaction progress. ● Stagnant, □ 100 rpm. The data presented are averages over three experiments for a 25 mM $CaCl_2$ solution.

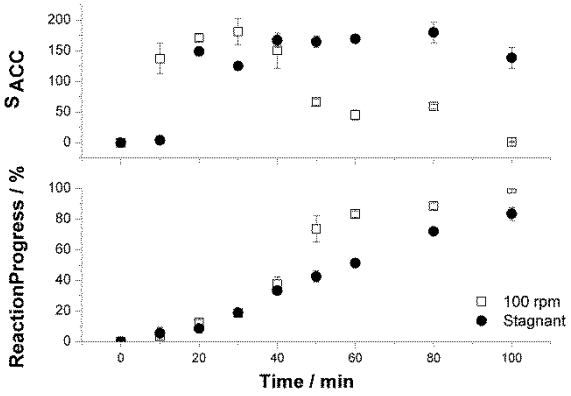

Figure 7. SEM images of calcite crystals produced using the ADM and the slow addition technique. (A) 1.25 mM Ca ADM, (B) 1.25 mM Ca Slow Addition, (C) 5 mM Ca ADM, (D) 5 mM Ca Slow Addition.

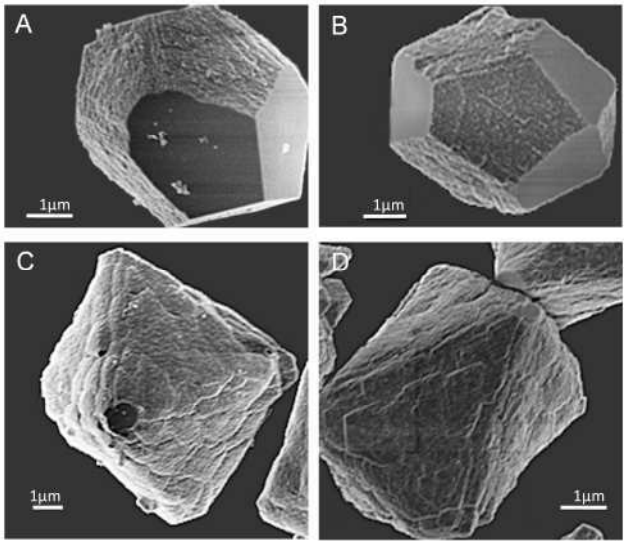

Table 1: Summary of ADM crystallization parameters under different experimental conditions, where (k_1) is the carbon accumulation rate in solution, (k_2) is the crystallization rate, (dC_T/dt) the total carbon addition rate, (dCO_3/dt) the carbonate addition rate, (t_{Ind}) the induction time and (S_{Ind}) is the supersaturation with respect to ACC at the induction point.

Experimental Condition	**k_1** [mM /min]	**k_2** [mM /min]	**dC_T/dt** [mM /min]	**dCO_3/dt** [mM /min]	**t_{Ind}** (mins)	**S_{Ind}** [*]	**Polymorph Distribution†** **Primary**	**Secondary**
Base Condition*	0.634±0.045	-0.228±0.007	0.849	0.138	15	31	Calcite	Vaterite
M ass $(NH_4)_2CO_3$								
5g	0.650±0.012	-0.224±0.038	0.864	0.140	16	30	Calcite	Vaterite
1.5g	0.654±0.095	-0.243±0.012	0.881	0.126	14	32	Calcite	Vaterite
$CaCl_2$ Concentration								
50mM	0.554±0.049	-0.464±0.025	1.019	0.090	20	150	Calcite	-
10mM	0.694±0.023	-0.120±0.008	0.814	0.225	10	13	Vaterite	Calcite
Solution Surface Area								
58cm^2	0.685±0.034	-0.320±0.001	1.034	0.176	10	40	Calcite	-
13cm^2	0.139±0.007	-0.072±0.011	0.223	0.050	33	10	Vaterite	Calcite
Sec. Diffusion Barrier Free Cross Sectional Area‡								
4cm^2	*0.089*±0.003	-0.056±0.006	0.156	0.063	35	40	Calcite	Vaterite
2cm^2	0.070±0.014	-0.037±0.005	0.107	0.014	47	50	Calcite	Vaterite
0.6cm^2	0.025±0.006	-0.008±0.002	0.0261	0.008	93	30	Vaterite	Calcite
Agitation								
100 rpm	1.047±0.080	-0.324±0.018	1.261	0.208	15	160	Calcite	Aragonite

*Base Condition (25mM $CaCl_2$, 70ml, 48cm^2, 3g $(NH_4)_2CO_3$, 2.6L overhead space, no secondary diffusion boundaries)
†Primary and Secondary Polymorph Constituent after 100min/‡200min estimated based on SEM Images, Raman- and IR-Spectra

The table of contents entry

Elucidation of the changes in solution which accompany $CaCO_3$ precipitation by the widely-used ammonia diffusion method enables replication of calcite mesocrystals via a simple and highly reproducible titration-based method. The experiments also demonstrate that aggregation-based growth, which generates these complex structures, is promoted by high and constant supersaturation levels, giving insight into the mechanisms of mesocrystal formation.

Keywords: Biomineralization• Biomimetics• Hierarchical Structures• Self-Assembly • Block Copolymers

Johannes Ihli, Pieter Bots, Alexander Kulak, Liane G Benning, Fiona C Meldrum *

Elucidating Mechanisms of Diffusion-Based Calcium Carbonate Synthesis Leads to Controlled Mesocrystal Formation

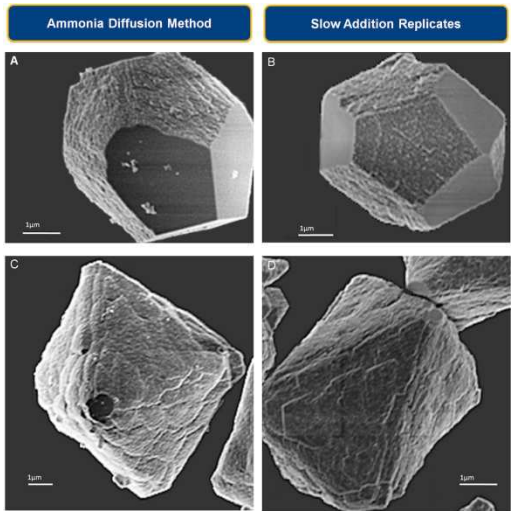

Elucidating Mechanisms of Diffusion-Based Calcium Carbonate Synthesis Leads to Controlled Mesocrystal Formation

Johannes Ihli, Pieter Bots, Alexander Kulak, Liane G Benning, Fiona C Meldrum

1. Materials and Methods

Experiments were performed where the changes in the solution composition accompanying $CaCO_3$ precipitation using the ammonia diffusion method (ADM) were characterized. The importance of certain key variables was also determined: the initial mass of ammonium carbonate, the initial calcium concentration, the solution surface area, the presence of a diffusion barrier and stirring of the solution. The insight gained was then used to achieve highly reproducible formation of calcium carbonate mesocrystals using a titration-based method.

1.1 Materials and General Preparative Methods

Ammonium carbonate, calcium chloride dihydrate and a 25 wt% solution of the sodium salt of poly(4-styrenesulfonic acid co-maleic acid) (PSS-MA) sodium salt were purchased in analytical grade from Sigma Aldrich and used without further purification. Solutions were prepared using Milli-Q Standard 18.2 MΩcm. Experiments were performed in triplicate, at room temperature, with solubility constants being adjusted accordingly.[1, 2]

1.2 Characterization of the Ammonia Diffusion Method

70 mL of calcium chloride solution (15-50 mM) in a crystallization dish with a solution surface area of 13-58 cm^2 was placed in a 2.6 L desiccator. A pH electrode, a temperature recorder and a tube through which the samples could be removed were inserted into the crystallization solution. Solid ammonium carbonate (1.5-5 g), thinly spread in a glass dish, was added to the chamber. This dish was either uncovered, or was covered with Parafilm to

provide a diffusion barrier, where the Parafilm was perforated to different degrees to give free surface areas of 0.6, 2 or 4 cm^2. The chamber was then sealed.

The changes in the reaction solution accompanying precipitation of $CaCO_3$ were evaluated by taking samples of volume 0.5 mL from the solution at intervals of 10 min. These were immediately diluted with 19.5 mL ethanol to replace water molecules adsorbed to the calcium carbonate surfaces and to prevent the solid from dissolving.[3] Next, 10.5 mL of Milli-Q water was then added to prevent further precipitation. 5 mL of the obtained mixture was centrifuged at 140 rpm for 90 seconds to separate the solution from the solid matter. The concentrations of aqueous calcium and carbon in the prepared solution were determined using atomic absorption spectroscopy (AA) and Ion chromatography (IC) respectively. For AA analyses, a 1 mL aliquot was dispensed into 4 mL of 5% nitric acid, and analysis was performed using a Perkin Elmer AA Analyst 400, operating with an oxy/acetylene flame. The total carbon content in the solution was determined by diluting 0.5 mL of the treated reaction solution with 1 mL of Milli-Q water. The resulting solution was then analyzed using a Dionex DX600 Ion chromatograph, equipped with Ion Pac AS15 column, using KOH as the eluent.

The experimental run time was limited to 100 min when no additional diffusion barriers were used and 200 min when further diffusion barriers were in place. The reaction was terminated by opening the reaction chamber, and the remaining solid ammonium carbonate was weighed. The weight loss of the ammonium carbonate ($\Delta(NH_4)_2CO_3$) and its molecular weight ($MW_{(NH4)2CO2}$) were then used in combination with the measured final carbon concentration in solution (C_T), the solution volume (V_L), the carbon concentration in the gas phase (V_{GP}), the expected equilibirum carbon dioxide vapor pressure (P_{CO2}) and the measured decrease in calcium concentration (ΔCa), to setup a carbon mass balance as a control indicator, Equation 1.

$$\frac{\Delta((NH_4)_2CO_3)_s}{MW_{(NH_4)_2CO_3}} = [\Delta Ca + C_T] * V_L + \frac{P_{CO_2}}{R * T} * V_{GP} \quad (1)$$

In a second set of experiments, the above setup was extended to determine the induction point by circulating the crystallizing solution through the beam path of a UV/VIS spectrophotometer in transmission mode (Perkin-Elkin Lambda 35 system λ= 500 nm) using a closed flow cell. Liquid transport to and from the flow cell/desiccator was performed using a double channel peristaltic pump.

1.3 Calculation of Carbonate Concentration, Supersaturation and Crystallization Progress

The solution carbonate concentrations (CO_3^{2-}, HCO_3^- and H_2CO_3) were calculated, based on the total inorganic carbon concentration (C_{TS}) and pH measurements,[4] using a simplified carbon mass balance and carbonic dissociation constants (K_A), as described in Equations 2-5. The required activity coefficients were calculated using the Davies equation and were found to be close to unity in diluted samples prior to analyzes.[5]

$$[C_{TS}] = [{CO_3}^{2-}] + [HCO_3^-] + [H_2CO_3] \quad (2)$$

$$[{CO_3}^{2-}] = \frac{[C_{TS}]\, K_{A_1}\, K_{A_2}}{[H^+]^2 + K_{A_1} * [H^+] + K_{A_1}\, K_{A_2}} \quad (3)$$

$$[HCO_3^-] = \frac{[C_{TS}]\, K_{A_1}\, [H^+]}{[H^+]^2 + K_{A_1}\, [H^+] + K_{A_1}\, K_{A_2}} \quad (4)$$

$$[H_2CO_3^*] = \frac{[C_{TS}]\, [H^+]}{[H^+]^2 + K_{A_1}\, [H^+]^2 + K_{A_1}\, K_{A_2}} \quad (5)$$

The crystallization progress (ξ) was determined by recording the total calcium concentration in solution, as described in Equation 6.

$$\xi = \left(\frac{Ca_t - Ca_i}{Ca_t - Ca_{equilibirum}} \right) \quad (6)$$

The calculated supersaturation (S) with respect to a specific polymorph (x), is expressed as the ratio of ionic activity product to solubility product (K_{sp}), as presented in Equation 8.

$$K_{sp_x} = a[Ca^{2+}]\ a[{CO_3}^{2-}] \quad (7)$$

$$S_x = \sqrt{\frac{a[Ca^{2+}]\ a[{CO_3}^{2-}]}{K_{sp_x}}} \quad (8)$$

1.4 Precipitation of Calcium carbonate Mesocrystals

In order to test whether the characterization of the ADM carbonate and supersaturation profiles could be translated to a diffusion-free experimental set-up, $CaCO_3$ mesocrystals were precipitated in the presence of poly(4-styrenesulfonic acid co-maleic acid) (PSS-MA) by drop-wise addition of reagents into solution under conditions which paralleled the ADM. The crystal morphologies were then compared with those prepared from identical reagents using the ADM.

Replication of the ADM was achieved by slow addition of $(NH_4)_2CO_3$ (100-300 mM) solution into a 250 mL crystallization dish containing 80 mL $CaCl_2$-PSS MA solution (1.5-5 mM $CaCl_2$, ~325 ppm PSS-MA). A syringe pump was used to slowly add the $(NH_4)_2CO_2$ to the crystallization dish under constant agitation with an orbital shaker. The addition rate and concentration of the $(NH_4)_2CO_3$ were determined based on the carbon addition rates derived

from the ADM. Cleaned glass slides were placed in the dish at the beginning of the experiment for subsequent SEM analysis of the crystals, and the dish was covered with Parafilm to prevent CO_2 exchange with the atmosphere. At the end of the experiment, the glass slides were removed from solution and were washed with Milli-Q water. While the reaction solution was rapidly vacuum filtered using a 0.45µm membrane filter, and the separated precipitates were washed with ~10 mL EtOH, before being left to dry in air.

The surface area of the $CaCO_3$ mesocrystals was determined using the method of Brunauer, Emmett and Teller (BET)[6] (Micrometrics ASAP 2020, Nitrogen Sorption). Thermogravimetric analysis (TGA) (TA Instruments STD Q600, 5 °C/min, 100 ml/min N_2) was applied to determine the polymer content in the crystals, while their morphologies were characterized using a LEO 1530 Gemini FEGSEM operating at 2.00 kV or a NeoScope JCM-5000 SEM operating at 10 kV. Crystal polymorphs were determined by Raman microscopy, using a Renishaw 2000 inVia-Raman microscope equipped with a 785 nm diode laser, or IR spectroscopy, using a Perkin Elmer Spectrum 100 FT-IR Spectrometer.

As a control, $CaCO_3$ mesocrystals were also precipitated using the traditional ADM, described by Equations 9-16, where 70 ml of a solution of 5-1.25 mM $CaCl_2$ and 325 ppm PSS-MA were placed in a crystallization dish with a surface area 48 cm^2, covered with a perforated Parafilm to provide an additional diffusion barrier with a 0.6 cm^2 of free surface area. The reaction was then carried out as described in section 2.2 using 3 g $(NH_4)_2CO_3$ and the solid products were sampled and analyzed as described above.

$$(NH_4)_2CO_{3_S} = H_2O_{\boldsymbol{g}} + CO_{2_{\boldsymbol{g}}} + 2NH_{3_{\boldsymbol{g}}} \quad (9)$$

$$[NH_3]_{\boldsymbol{g}} = [NH_3]_{\boldsymbol{aq}} \quad (10)$$

$$[NH_3]_{AQ} + H_2O = [NH_4{}^+] + [OH^-] \quad (11)$$

$$[CO_2]_G = [CO_2]_{AQ} \tag{12}$$

$$[CO_2]_{AQ} + H_2O = [H_2CO_3] \tag{13}$$

$$[H_2CO_3] = [HCO_3^-] + [H^+] \tag{14}$$

$$[HCO_3^-] = \left[CO_3^{2-}\right] + [H^+] \tag{15}$$

$$\left[CO_3^{2-}\right] + [Ca^{2+}] = CaCO_{3_S} \tag{16}$$

2. Ammonia Diffusion Method –Solution Composition Calculation & Supporting Results

2.1 Calculation of Equilibrium Constants (Equations 17-30)

The solution supersaturation, the calcium and carbonate concentrations were determined using the temperature (T)-dependent equilibrium constants (K), Henry (k_H) and carbonic acid-dissociation constants (K_A) as given below.[2, 7]

$$K_W = [OH^-][H^+] = 10^{-(-0.0261\cdot(T-273)+14.583)} \tag{17}$$

$$k_{H_{CO_2}} = \frac{Pco_2}{[CO_2]_{(aq)}} = 10^{-\left(108.386+0.0198507T-\frac{6919.53}{T}-40.4515\log_{10}(T)+\left(\frac{669365}{T^2}\right)\right)} \tag{18}$$

$$K_{A_1} = \frac{[H^+][HCO_3^-]}{[H_2CO_3^*]} = 10^{\left(\frac{-356.3094-0.06091964T+21834.37}{T}+126.833\log_{10}(T)-\frac{1684915}{T^2}\right)} \tag{19}$$

$$K_{A_2} = \frac{[H^+]\left[CO_3^{2-}\right]}{[HCO_3^-]} = 10^{\left(-171.9065-0.077993T+\frac{2839.319}{T}+71.595\log_{10}(T)\right)} \tag{20}$$

$$k_{H_{NH_3}} = \frac{P_{NH_3}}{[NH_3]_{(aq)}} = e^{\left(-8.09694+\left(\frac{3917.507}{T}\right)-0.00314T\right)} \quad (21)$$

$$K_{NH_4} = \frac{[H^+][NH_3]}{[NH_4{}^+]} = 10^{-\left(14+\cdot\log_{10}\left(e^{-16.97-\left(\frac{4411.025}{T}\right)-0.044T}\right)\right)} \quad (22)$$

$$K_{CaHCO_3} = \frac{[CaHCO_3{}^+]}{[Ca^{2+}][HCO_3{}^-]} = 10^{\left(-1209.12+0.31294T-\left(\frac{34765.05}{T}\right)-478.782\log_{10}(T)\right)} \quad (23)$$

$$K_{CaCO_{3aq}} = \frac{[Ca^{2+}][CO_3{}^{2-}]}{[CaCO_3]^0} = 10^{-\left(-1228.732-0.299444T+\frac{35512.75}{T}+485.818\log_{10}(T)\right)} \quad (24)$$

$$\log_{10} K_{CaOH} = 25.12 \quad (25)$$

$$\log_{10} K_{Ca(OH)_2} = 22.80 \quad (26)$$

2.2 Temperature-Dependence of the Solubility Products of the $CaCO_3$ Polymorphs (K_{sp})

$$K_{sp_{Calcite}} = 10^{\left(-171.9065-0.077993T+\frac{2839.319}{T}+71.595\log_{10}(T)\right)} \quad (27)$$

$$K_{sp_{Aragonite}} = 10^{\left(-171.9773-0.0779931T+\frac{2903.293}{T}+71.595\log_{10}(T)\right)} \quad (28)$$

$$K_{sp_{Vaterite}} = 10^{\left(-172.1295-0.0779933T+\frac{3074}{T}+71.595\log_{10}(T)\right)} \quad (29)$$

$$K_{sp_{ACC}} = 10^{-\left(0.0001(T+273)^2+0.0041(T+273)+6.2272\right)} \quad (30)$$

2.3 Solution Activity Coefficients (f)

Solution activities were calculated using the Davies equation, based on the measured ionic strength of the solution as recalculated from diluted samples analyzed.[5]

Ionic strength (I)

$$I = \frac{1}{2} \cdot \sum c_i \, z_i^2 \tag{31}$$

Davies Equation

$$-\log_{10}(f) = 0.5 \, z_1 \, z_2 \left(\frac{\sqrt{I}}{1+\sqrt{I}} - 0.30 \, I \right) \tag{32}$$

z_i = charge of ionic species considered

2.4 Calculation of the Equilibrium Solution Composition (Equations 33-40)

The final solution composition was calculated using the charge balance given below as a function of the vapour pressure of the ammonium carbonate.

The ***underlying charge balance*** gives the following:

$$2[Ca^{2+}]+[H^+]+[NH_4^+]+[HCaCO_3^+]=[OH^-]+[HCO_3^-]+2[CO_3^{2-}]+[Cl^-] \tag{33}$$

This was then solved via ***Newton's method[4]:***

$$\begin{aligned} = [H^+]^4 \cdot \left(\frac{2 \cdot K_{sp} \cdot k_{H_{CO_2}}}{K_{A_1} \cdot K_{A_2} \cdot P_{CO_2}} \right) + [H^+]^3 + [H^+]^3 \cdot \left(\frac{P_{NH_3}}{K_{NH_4} \cdot k_{H_{NH_3}}} \right) + [H^+]^3 \\ \cdot \left(\frac{K_{sp} \cdot K_{CaHCO_3}}{K_{A_2}} \right) \\ -[H^+]^2 \cdot [Cl^-] - [H^+] \, K_W - [H^+] \cdot \frac{P_{CO_2} \cdot K_{A_1}}{k_{H_{CO_2}}} - 2 \cdot \left(\frac{K_{A_1} \, K_{A_2} \, P_{CO_2}}{k_{H_{CO_2}}} \right) \end{aligned} \tag{34}$$

$$[H_2CO_3{}^*] = \frac{P_{CO_2}}{k_{H_{CO_2}}} \tag{35}$$

$$[HCO_3{}^-] = \frac{P_{CO_2}\, k_{H_{CO_2}} K_{A_1}}{[H^+]} \tag{36}$$

$$[CO_3{}^{2-}] = \frac{P_{CO_2}\, k_{H_{CO_2}} K_{A_1}\, K_{A_2}}{[H^+]^2} \tag{37}$$

$$[NH_3] = \frac{P_{NH_3}}{k_{H_{NH_3}}} \tag{38}$$

$$[NH_4{}^+] = \frac{[H^+][NH_3]}{K_{NH_4}} \tag{39}$$

$$[Ca_i{}^{2+}] = \frac{K_{sp_i}}{[CO_3{}^{2-}]} \tag{40}$$

2.5 Calculation of the Solution Composition (Equations 41-45)

The actual concentrations of the species present in solution were calculated based on time-resolved measurements of pH, temperature, calcium concentration, the total content of nitrogen (N_T) and carbonates (C_{TS}) present in solution, using the equations given below.

$$[CO_3{}^{2-}] = \frac{[C_{TS}]\ K_{A_1} K_{A_2}}{[H^+]^2 + K_{A_1}[H^+] + K_{A_1} K_{A_2}} \tag{41}$$

$$[HCO_3{}^-] = \frac{[C_{TS}]\, K_{A_1}[H^+]}{[H^+]^2 + K_{A_1}[H^+] + K_{A_1} K_{A_2}} \tag{42}$$

$$[H_2CO_3{}^*] = \frac{[C_{TS}][H^+]^2}{[H^+]^2 + K_{A_1}[H^+] + K_{A_1}K_{A_2}} \quad (43)$$

$$[NH_4{}^+] = \frac{[N_T][H^+]}{[H^+] + \left(\frac{K_W}{K_{NH_4}}\right)} \quad (44)$$

$$[NH_3] = \frac{[N_T]\left(\frac{K_W}{K_{NH_4}}\right)}{[H^+] + \left(\frac{K_W}{K_{NH_4}}\right)} \quad (45)$$

Figure S1. A time-resolved UV/Vis spectrum showing the change in transmittance/ turbidity occurring during $CaCO_3$ precipitation using the ammonia diffusion method. IR analysis of samples isolated at key times in the reaction were (A) amorphous calcium carbonate (ACC), (B) vaterite and (C) calcite. Here, the peak at 747 cm^{-1} is a fingerprint for vaterite, while the peak at 712 cm^{-1} identifies calcite.

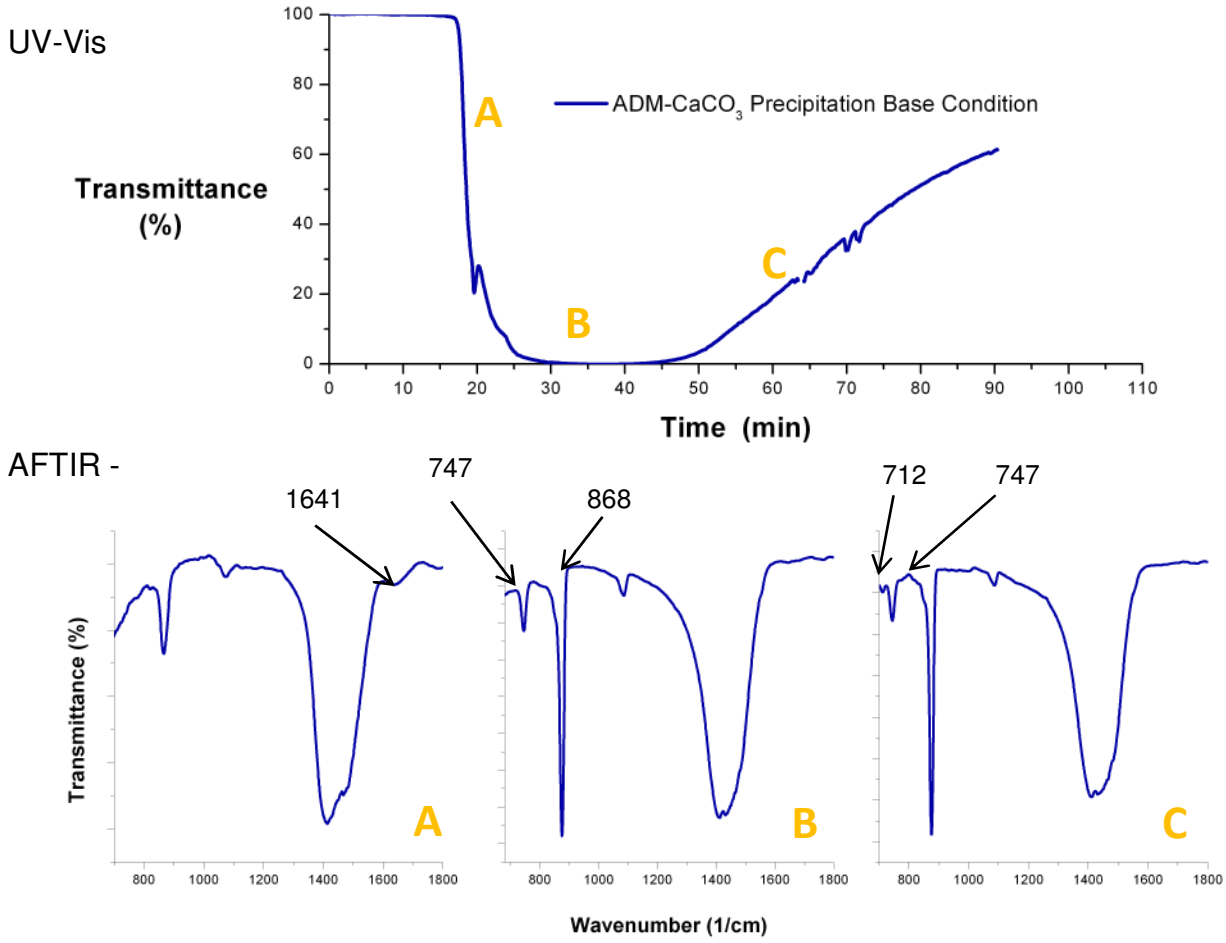

Figure S2: A typical pH profile for an ADM experiment (70 mL, 25 mM $CaCl_2$, A = 48 cm^2, 3 g ammonium carbonate, 2.6 L head space, no additional diffusion boundaries) which shows the establishment of a constant solution pH (9.25) after 20 hours.

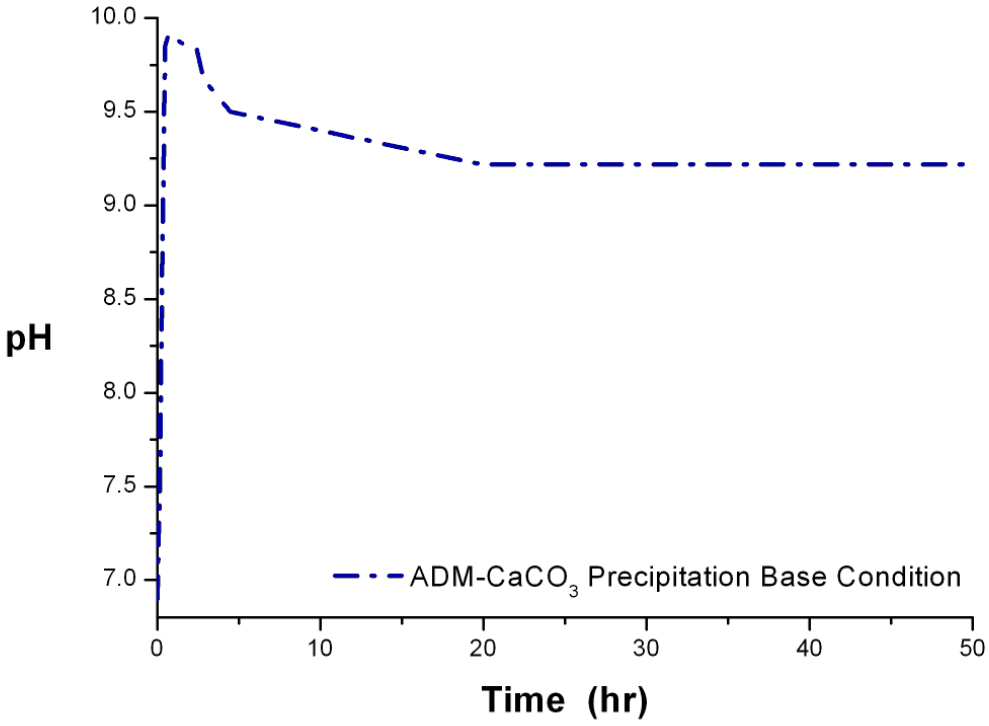

Figure S3: Time-resolved profiles of calcium carbonate precipitation experiments using the ammonia diffusion method, studying the influence of changes in initial amounts of ammonium carbonate added (1.5g, 3g and 5g). Experimental conditions 70 mL of 25 mM $CaCl_2$, 48 cm^2 surface area, 2.6 L head space, no additional diffusion barriers).— 1.5 g, --- 3 g, -•- 5g, ▲ 1.5g, •3g, ■ 5g $(NH_4)_2CO_3$.

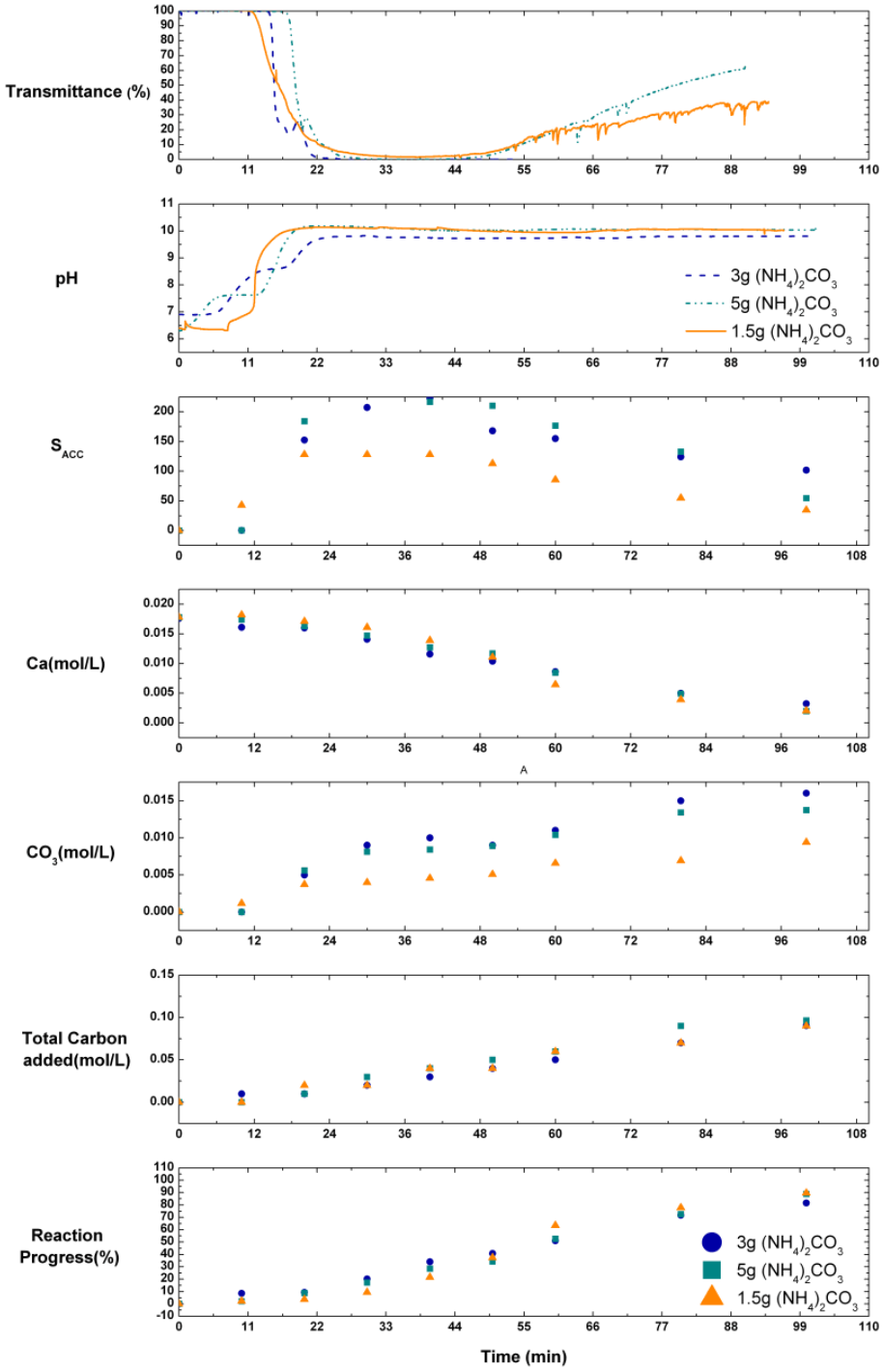

Figure S4: SEM images of calcium carbonate precipitates obtained via the ammonia diffusion method after 100 minutes under reaction conditions of 70 mL, 3 g ammonium carbonate, 48 cm^2, 2.6 L head space, no additional diffusion boundaries and (A) 25 mM $CaCl_2$, no agitation, (B) 25 mM $CaCl_2$ and 100 rpm agitation, (C) 50 mM $CaCl_2$, no agitation, (D) 10 mM $CaCl_2$, no agitation.

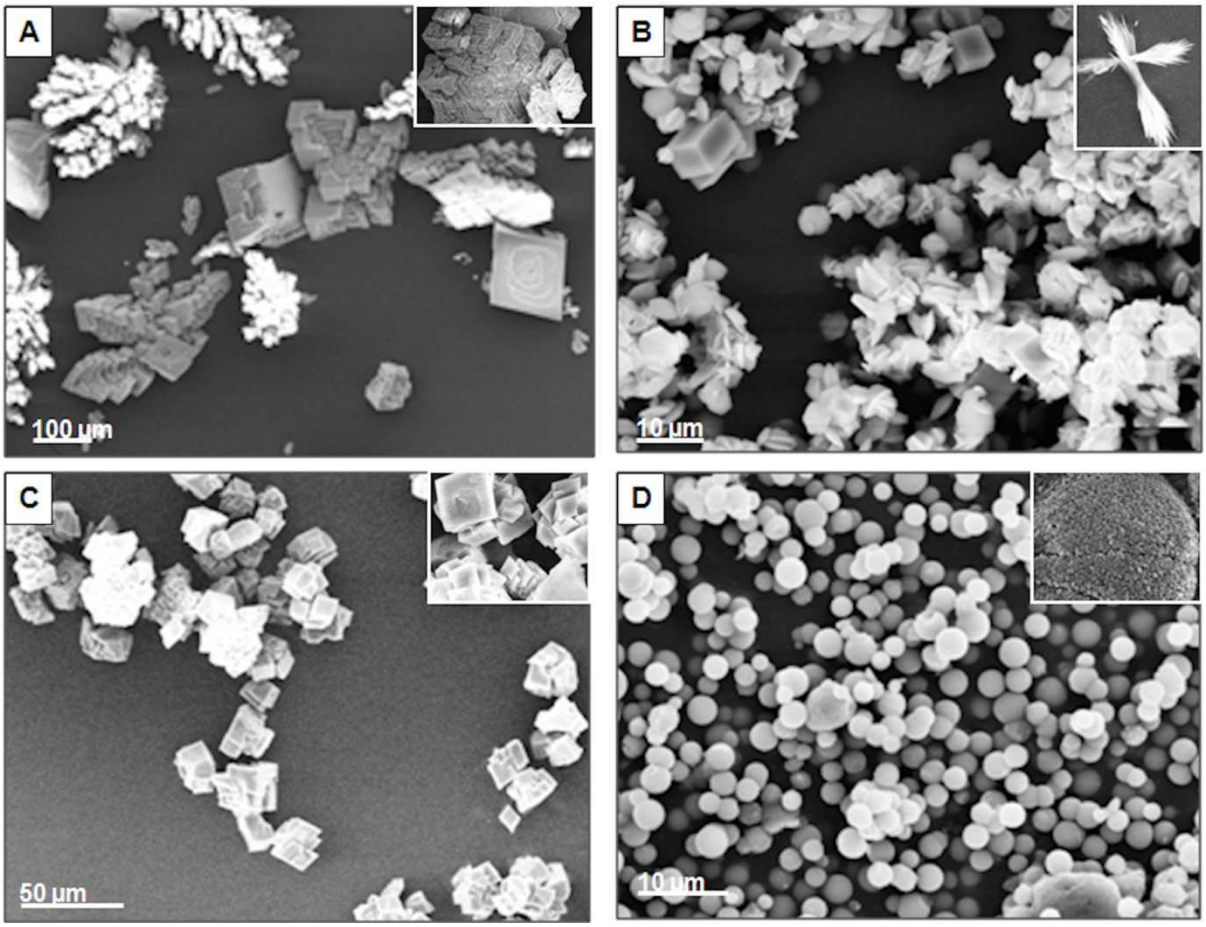

Figure S5: Raman spectra of calcium carbonate precipitates obtained via the ammonia diffusion method under reaction conditions of 70 mL, 3 g ammonium carbonate, 48 cm^2, 2.6 L, no additional diffusion boundaries and (A) 25 mM $CaCl_2$, no agitation (Calcite+Vaterite), (B) 25 mM $CaCl_2$ and 100 rpm agitation (Calcite+Aragonite), (C) 50 mM $CaCl_2$, no agitation (Calcite), (D) 10 mM $CaCl_2$, no agitation (Vaterite+Calcite). The $CaCO_3$ polymorphs can be identified based on characteristic peaks, where peaks at 1085, 711, 281 and 155 cm^{-1} identify calcite, peaks at 1085, 705, 701, 208 and 155 cm^{-1} identify aragonite and peaks at 1093, 1066, 753, 713 and 300 cm^{-1} identify vaterite.[8]

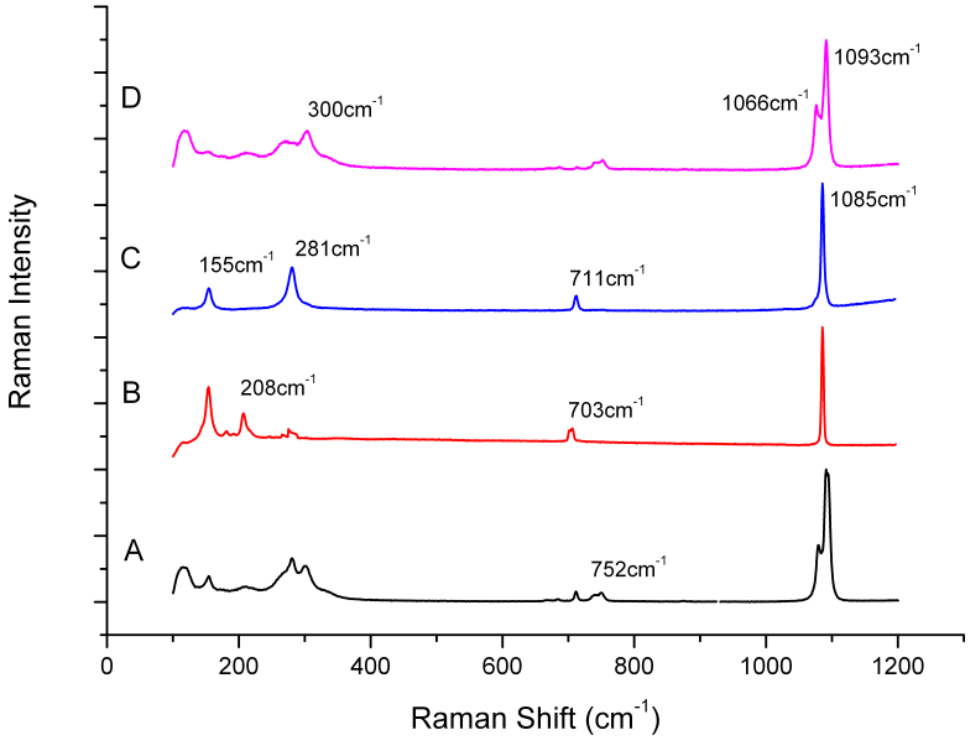

Figure S6: Time-resolved profiles of calcium carbonate precipitation experiments using the ammonia diffusion method studying the influence of initial $CaCl_2$ concentration (10 mM, 25 mM and 50 mM). Experimental conditions 70 mL of x mM $CaCl_2$, 3 g $(NH_4)_2CO_3$, 48 cm^2 surface area, 2.6 L head space, no additional diffusion barriers).—10mM, --- 25mM, -•- 50mM, ▲ 10mM, • 25mM, ■ 50mM $CaCl_2$.

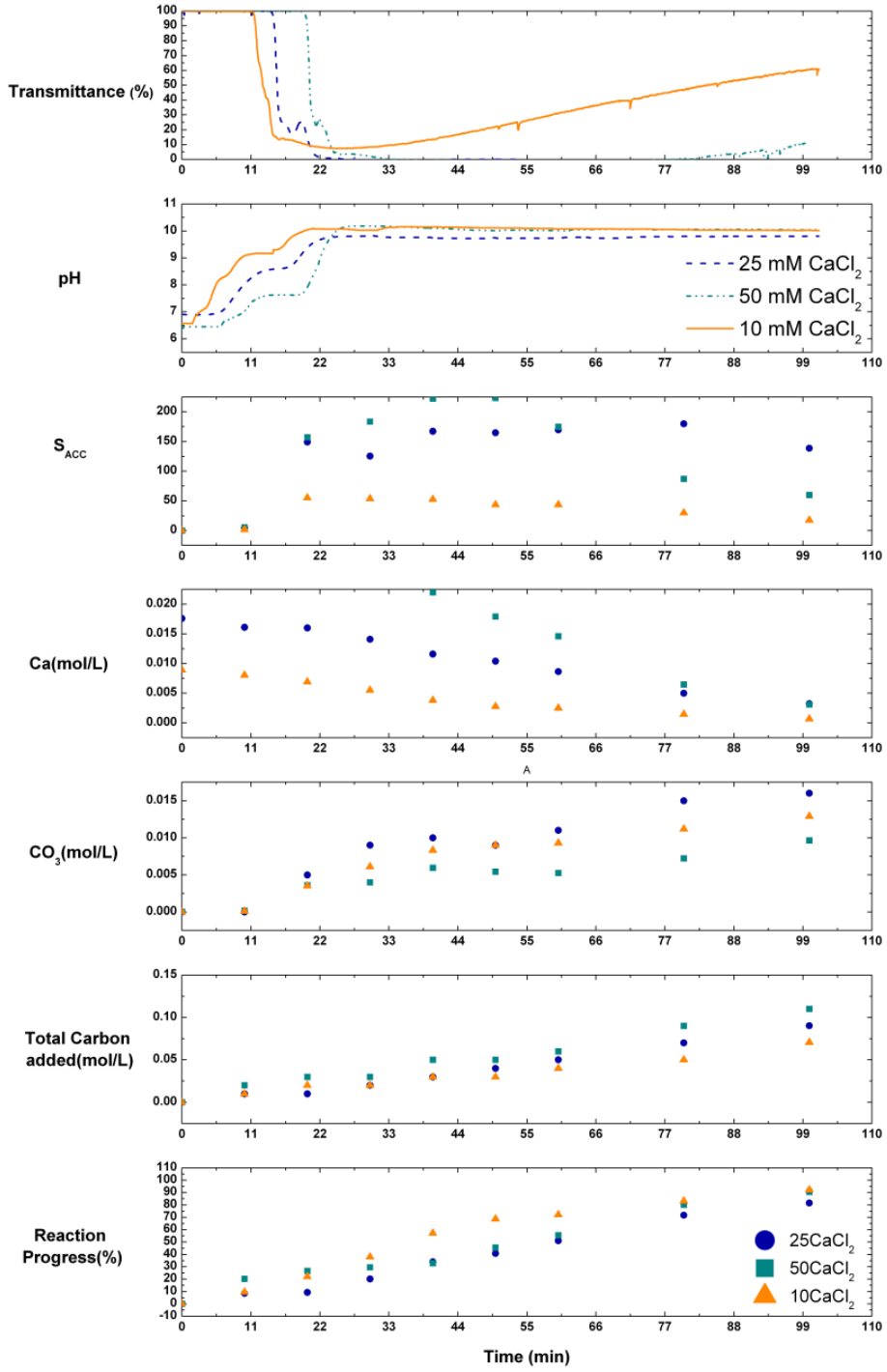

Figure S7: Time-resolved profiles of calcium carbonate precipitation experiments using the ammonia diffusion method studying the influence of solution surface areas (13 cm^2, 48 cm^2,

58 cm^2). Experimental conditions 70 mL of 25 mM $CaCl_2$, 3 g $(NH_4)_2CO_3$, x cm^2 surface area, 2.6 L head space, no additional diffusion barriers).—13cm^2, --- 48cm^2, -•- 58cm^2, ▲ 13cm^2, • 48cm^2, ■ 58cm^2.

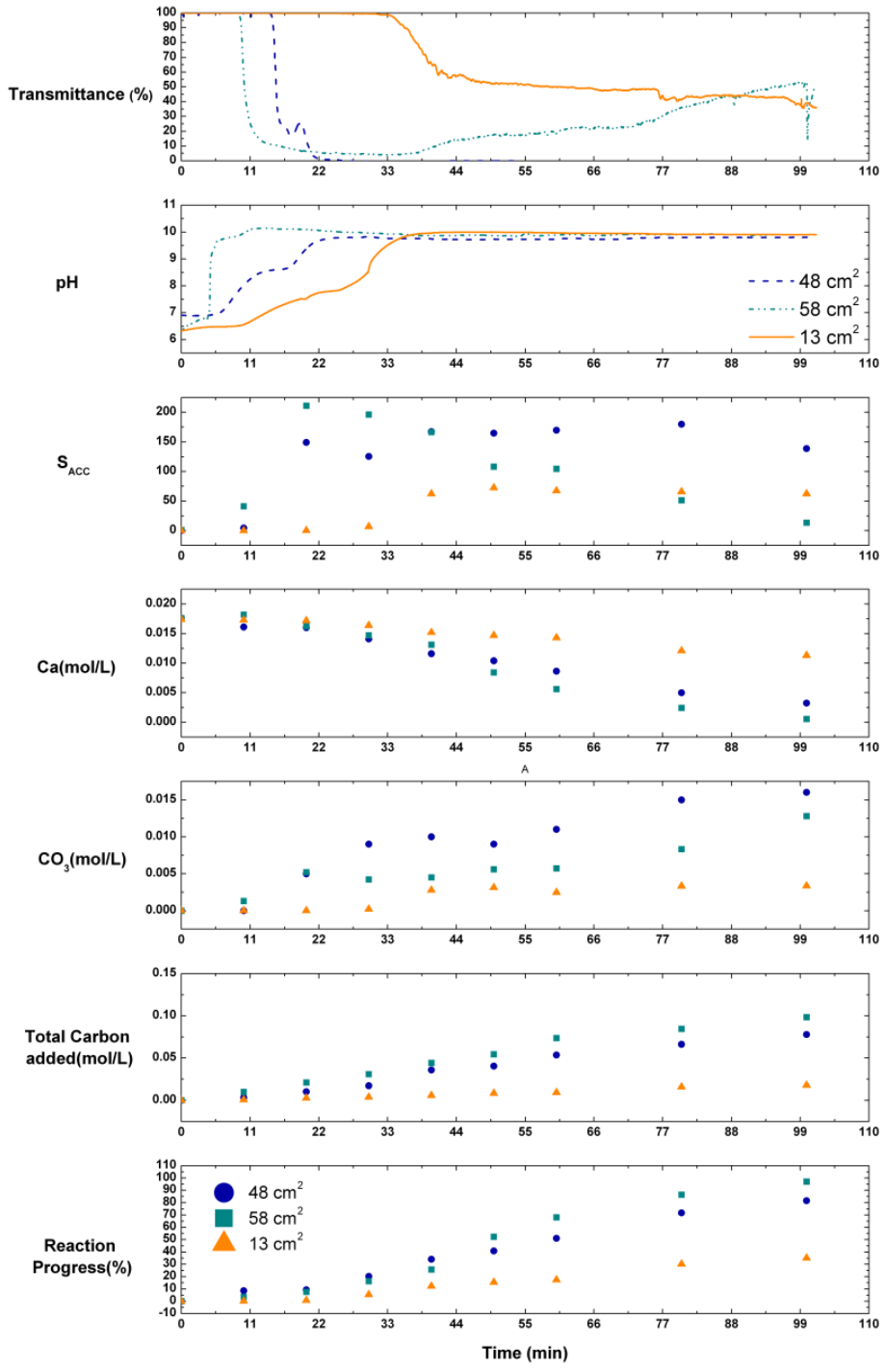

Figure S8: Time-resolved profiles of calcium carbonate precipitation experiments using the ammonia diffusion method studying the effect of solution agitation (100 rpm). Reaction conditions 70 mL of 25 mM $CaCl_2$, 48 cm^2 surface area, 3g ammonium carbonate, 2.6 Liter head space, no additional diffusion barriers). — Stirring 100 rpm, --- Stagnant, ■ Stirring 100 rpm, •Stagnant.

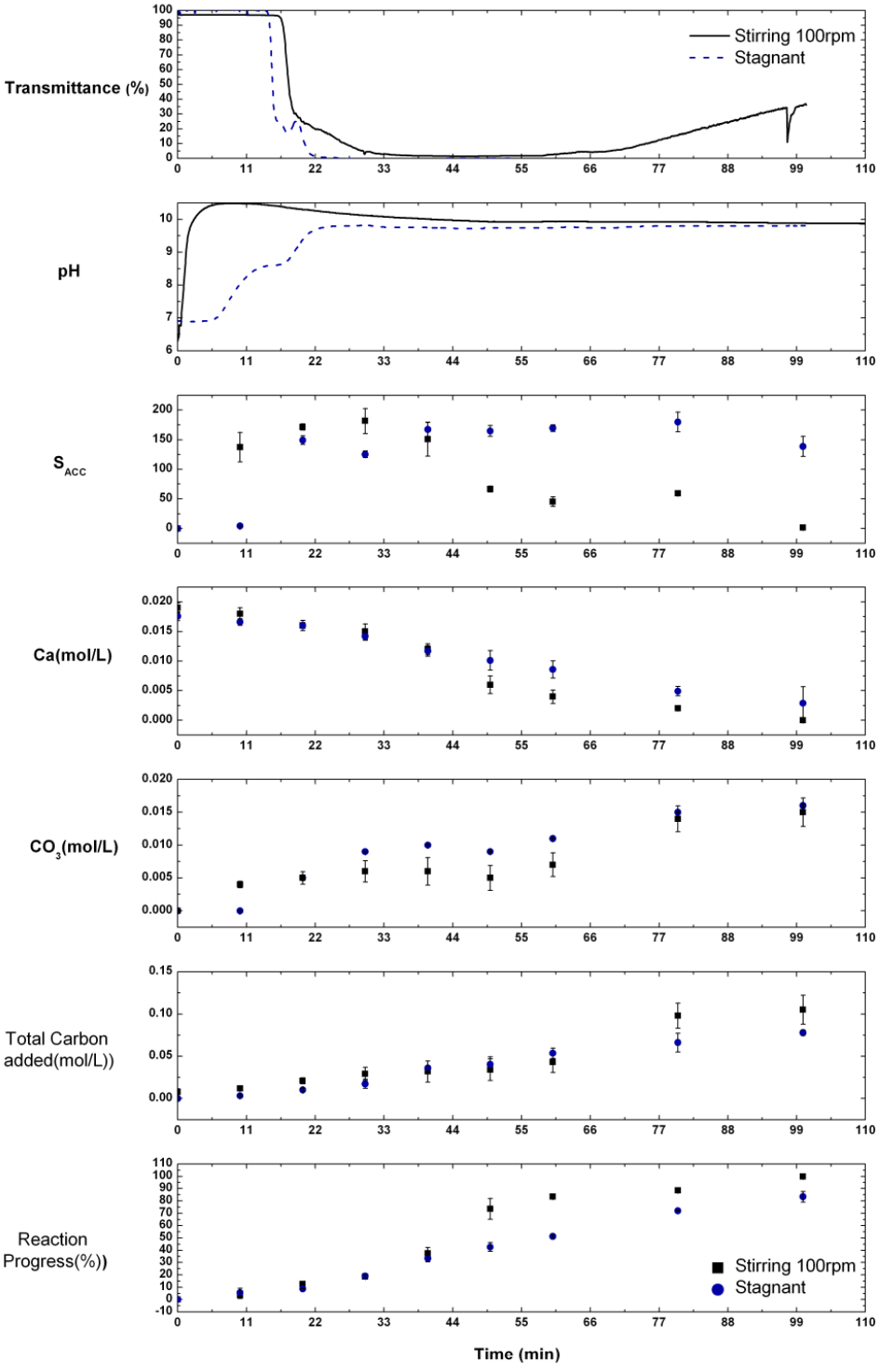

3. Characterization of $CaCO_3$-PSS MA Mesocrystal

Figure S9: (A) Raman spectrum and (B) IR spectra of pseudo-octahedral $CaCO_3$ mesocrystals obtained in the presence of PSS-MA, and (C) Raman spectrum and (D) IR spectrum of rhombohedral calcite crystals.

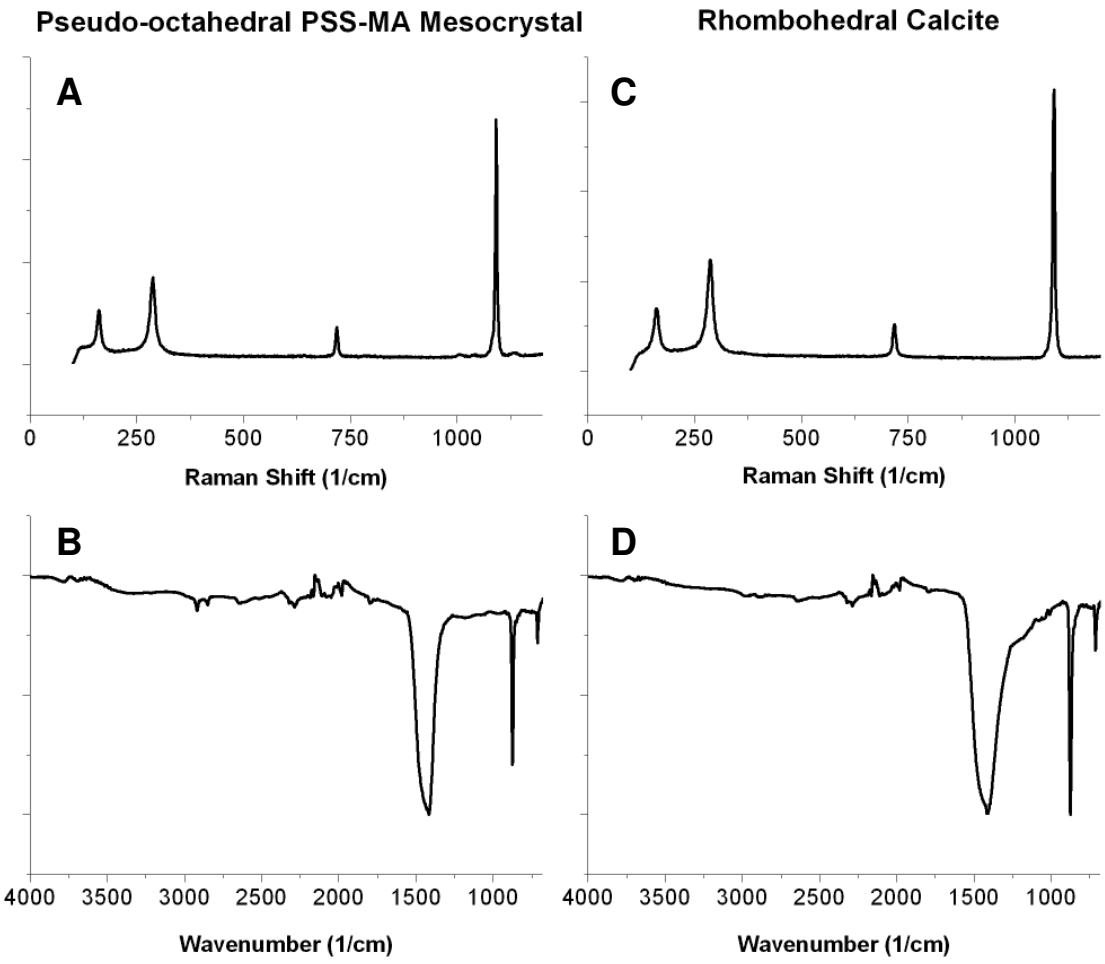

Figure S10: TGA spectra of pseudo-octahedral $CaCO_3$ mesocrystals produced in the presence of PSS-MA by slow addition of reagents. A heating rate of 5 °C/min was applied.

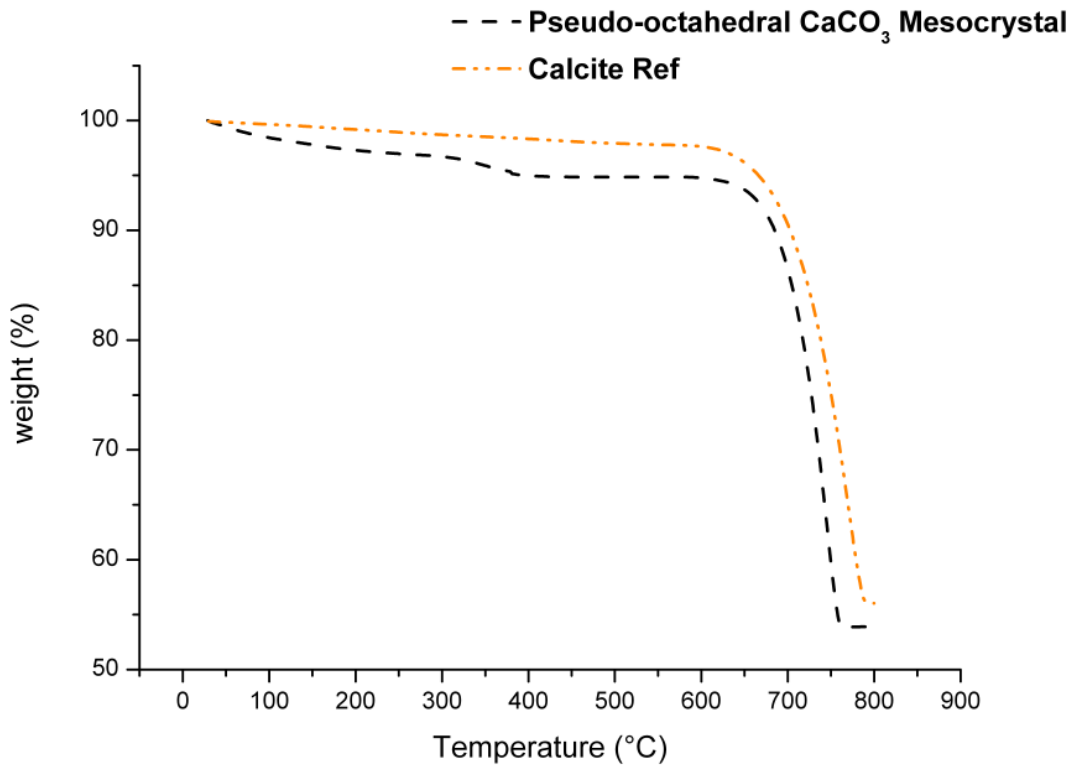

4. References

[1] J. R. Clarkson, T. J. Price, C. J. Adams, Journal of the Chemical Society, Faraday Transactions **1992**, 88, 243.

[2] M. Donnet, P. Bowen, LemaI, J. tre, J Colloid Interf Sci **2009**, 340, 218; L. N. Plummer, E. Busenberg, Geochim Cosmochim Ac **1982**, 46, 1011.

[3] L. Zhang, L.-H. Yue, F. Wang, Q. Wang, J. Phys. Chem. B **2008**, 112, 10668; D. J. Cooke, R. J. Gray, K. K. Sand, S. L. S. Stipp, J. A. Elliott, Langmuir **2010**, 26, 14520; K. K. Sand, M. Yang, E. Makovicky, D. J. Cooke, T. Hassenkam, K. Bechgaard, S. L. S. Stipp, Langmuir **2010**, 26, 15239.

[4] H. L. Bohn, B. McNeal, G. O'Connor, in *Soil Chemistry*, John Wiley Sons, **1985**, 316.

[5] C. W. Davies, *Ion Association*, Butterworths, London **1962**

[6] S. Brunauer, P. H. Emmett, E. Teller, J. Am. Chem. Soc. **1938**, 60, 309.

[7] E. Busenberg, L. N. Plummer, Geochimica Et Cosmochimica Acta **1985**, 49, 713; J. Y. Gal, J. C. Bollinger, H. Tolosa, N. Gache, Talanta **1996**, 43, 1497; L. Brecevic, A. E. Nielsen, J Cryst Growth 1989, 98, 504; A. P. Collier, M. J. Hounslow, AIChE Journal **1999**, 45, 2298.

[8] U. Wehrmeister, A. L. Soldati, D. E. Jacob, T. Häger, W. Hofmeister, J Raman Spectrosc **2010**, 41, 193.